Available online at www.sciencedirect.com
ScienceDirect
Remote Sensing of Environment 106 (2007) 285–304
Remote Sensing of Environment
www.elsevier.com/locate/rse

Regional evaporation estimates from flux tower and MODIS satellite data

Helen A. Cleugh [a,*], Ray Leuning [a], Qiaozhen Mu [b], Steven W. Running [b]

[a] CSIRO Marine and Atmospheric Research, PO Box 1666, Canberra, ACT, 2601, Australia
[b] Numerical Terradynamics Simulation Group, University of Montana, Missoula, MT 59812, USA

Received 14 November 2005; received in revised form 5 July 2006; accepted 15 July 2006

Abstract

Two models were evaluated for their ability to estimate land surface evaporation at 16-day intervals using MODIS remote sensing data and surface meteorology as inputs. The first was the aerodynamic resistance–surface energy balance model, and the second was the Penman–Monteith (P–M) equation, where the required surface conductance is estimated from remotely-sensed leaf area index. The models were tested using 3 years of evaporation and meteorological measurements from two contrasting Australian ecosystems, a cool temperate, evergreen *Eucalyptus* forest and a wet/dry, tropical savanna. The aerodynamic resistance–surface energy balance approach failed because small errors in the radiative surface temperature translate into large errors in sensible heat, and hence into estimates of evaporation. The P–M model adequately estimated the magnitude and seasonal variation in evaporation in both ecosystems (RMSE = 27 W m^{-2}, R^2 = 0.74), demonstrating the validity of the proposed surface conductance algorithm. This, and the ability to constrain evaporation estimates *via* the energy balance, demonstrates the superiority of the P–M equation over the surface temperature-based model. There was no degradation in the performance of the P–M model when gridded meteorological data at coarser spatial (0.05°) and temporal (daily) resolution were substituted for locally-measured inputs.

The P–M approach was used to generate a monthly evaporation climatology for Australia from 2001 to 2004 to demonstrate the potential of this approach for monitoring land surface evaporation and constructing monthly water budgets from 1-km to continental spatial scales.
© 2006 Elsevier Inc. All rights reserved.

Keywords: Land surface evaporation; Flux towers; MODIS remote sensing

1. Introduction

The ability to monitor evaporation[1] from land surfaces is important for applications requiring spatially-resolved estimates of moisture availability over large areas continuously at weekly to monthly timescales. Examples of such applications include irrigation scheduling (e.g. Dodds et al., 2005), managing carbon, water and land resources (e.g. Meyer, 1999; Raupach, 2001), and risk assessments for bushfires, dust storms and flooding. Evaporation is a large component of the terrestrial water balance, so improving the accuracy of evaporation estimates will significantly reduce uncertainties in terrestrial water balance modelling and improve the quality of information used in these applications.

Hydrometeorologists have striven for decades to use the global coverage of satellite-based remote sensing to provide accurate estimates of evaporation at daily to weekly time scales and at fine spatial scales (10^0 to 10^3 m). These efforts have been hindered by two problems: firstly, that the quantities of interest, such as carbon and water fluxes and their associated stores, must be estimated indirectly using algorithms that relate measured radiances to, for example, leaf area index (Myneni et al., 2002), gross and net primary productivity (Running et al., 2004), vegetation indices (Huete et al., 2002) and land surface temperature (Wan et al., 2002). Secondly, one of the biggest impediments to global, multi-temporal satellite-based monitoring is the conflicting requirement for algorithms that are biophysically realistic yet simple enough for global parameterisation and implementation. Zhao et al. (2005) demonstrates this for the MODIS primary productivity products, while a global MODIS evaporation product remains elusive because no

* Corresponding author.
E-mail address: Helen.Cleugh@csiro.au (H.A. Cleugh).
[1] In this paper, the term evaporation includes evaporation from water and soil, and transpiration from plants.

0034-4257/$ - see front matter © 2006 Elsevier Inc. All rights reserved.
doi:10.1016/j.rse.2006.07.007

algorithm has yet been found that achieves the right balance between accuracy and simplicity.

We present a new approach to building a global land surface evaporation algorithm using optical/thermal satellite data. Our goal is to develop an observation model appropriate for global implementation and routine monitoring of landscape-scale evaporation at weekly to monthly timescales. In this paper we use data products from the MODIS Moderate Resolution Imaging Spectroradiometer on the polar-orbiting Terra satellite, which has a daily overpass at around 10:30 h local time. With these constraints, the following model attributes are required:

i) Model inputs and parameters must be routinely available at daily time and local space scales, for large regions such as continental Australia, and globally.
ii) The model needs to be robust, i.e. evaporation estimates are constrained by energy and mass conservation and have relatively low sensitivity to the input data and parameters.
iii) The model needs to be insensitive to constraints imposed by the once-daily overpass of the polar orbiting satellite and the necessary cloud screening and compositing procedures.
iv) The model needs to be validated using comparable evaporation measurements from a diverse range of bioclimates.

These objectives are consistent with the ultimate goal for Fluxnet (Baldocchi et al., 2001), which seeks to integrate flux and concentration measurements, remote sensing and land-surface modelling to yield a comprehensive global biosphere monitoring network (Running et al., 1999; Zhao et al., 2005). Fluxnet encompasses over 400 towers distributed across the globe, providing hourly measurements of carbon, water and sensible heat fluxes across a diverse range of ecosystems and climates for multiple years (Baldocchi et al., 2001; http://www.daac.ornl.gov/FLUXNET/fluxnet.html). The insights and constraints provided by the simultaneous measurement of these fluxes and their corresponding scalar fields ensures that Fluxnet provides an excellent data set for land surface model development and testing. Data from two Australian flux stations (Ozflux: http://www.dar.csiro.au/lai/ozflux/) are used in this paper to test two evaporation models: i) an aerodynamic resistance–surface energy balance model and ii) the Penman–Monteith (P–M) equation, where the required surface conductance is estimated from remotely-sensed vegetation indices (leaf area index and NDVI).

The plan of the paper is as follows: Section 2 presents the fundamental energy balance and evaporation equations that underpin the evaporation modelling approaches that are tested; Section 3 describes the micrometeorological flux measurements used to develop and test the models; and Section 4 evaluates the two modelling approaches. Sections 5 and 6 then implement the successful model to determine monthly evaporation fluxes at 1-km resolution for the Australian continent. This demonstrates the potential to monitor monthly land surface evaporation at the regional-scale by combining surface-based meteorological measurements with MODIS remote sensing.

2. Modelling land surface evaporation

Energy partitioning at the surface of the earth is governed by the following three coupled equations:

$$H = \rho c_p \frac{T_s - T_a}{R_a}, \tag{1}$$

$$\lambda E = \frac{\rho c_p}{\gamma} \frac{e_s - e_a}{R_a + R_s}, \tag{2}$$

$$A = R_n - G - \Delta S = H + \lambda E, \tag{3}$$

where H, λE and A are the fluxes of sensible heat, latent heat and available energy, R_n is net radiation, G is soil heat flux; ΔS is the heat storage flux; T_s, T_a are the aerodynamic surface and air temperatures; e_s, e_a are the water vapour pressure at the evaporating surface and in the air; R_a is the aerodynamic resistance, R_s is the surface resistance to evaporation, λ is the latent heat of evaporation, ρ is air density, and c_p is the specific heat capacity of air. The psychometric constant γ is given by $\gamma = (M_a/M_v)(c_p P_a/\lambda)$, where M_a and M_v are the molecular masses of dry air and water vapour and P_a is atmospheric pressure.

These fundamental equations form the basis of a suite of land surface evaporation modelling approaches that use remotely-sensed radiances and are described in detail in several excellent reviews, for example Su (2005), Norman et al. (1995) and Caparrini et al. (2003). These reviews reveal several classes of remote sensing evaporation models, with the main operational approaches being: SEBAL (Bastiaanssen et al., 1998a,b); SEBS (Su, 2002); NTDI (McVicar & Jupp, 1999, 2002); the resistance surface energy balance (RSEB; Kalma & Jupp, 1990); the triangle method (Gillies & Carlson, 1995; Nemani & Running, 1989; Nishida et al., 2003); and the dual-source model developed by Norman et al. (1995) and Kustas and Norman (1999) that uses multi-angular remote sensing. Core to all of these approaches is the use of radiative surface temperatures (T_{sR}) to determine the surface energy balance *via* Eqs. (1)–(3). Recalling the required model attributes for a global evaporation algorithm, we evaluate the RSEB method and compare its performance to a new method based on the Penman–Monteith equation that eliminates surface temperature and uses remotely sensed vegetation indices such as leaf area index (Λ) to inform the model of the water availability of the land surface.

The next section describes these approaches in more detail while Section 4 assesses which model provides the best and most reliable estimates evaporation at multiple time and space scales.

2.1. Resistance–surface energy balance model

The resistance energy balance method calculates the flux of sensible heat from Eq. (1) by substituting the remotely-sensed radiative surface temperature (T_{sR}) for T_s, using the measured air temperature (T_a) and calculating the aerodynamic resistance (R_a) from:

$$R_a = \frac{1}{k^2 U}\left[\ln\left(\frac{z-d}{z_{0H}}\right) - \Psi_H\left(\frac{z-d}{L}\right)\right]\left[\ln\left(\frac{z-d}{z_0}\right) - \Psi_M\left(\frac{z-d}{L}\right)\right]. \tag{4}$$

In this equation k is von Karman's constant (0.4); U is wind speed at the reference height z; d is the zero-plane displacement height; z_0, z_{0H} are the roughness lengths for momentum and sensible heat, respectively; and Ψ_M, Ψ_H are the stability correction functions for momentum and heat which depend on the Monin–Obukhov length L (Kaimal & Finnigan, 1994). λE is then calculated as the residual of the energy balance using Eq. (3).

This approach has received much attention in the literature (e.g. Cleugh & Dunin, 1995; Hall et al., 1992; Kalma & Jupp, 1990) and its performance has been shown to be unreliable for some, or all, of the following reasons: i) the sensible heat flux predicted from (1) is not constrained by the requirement for energy conservation at the surface; ii) the aerodynamic and radiative surface temperatures are not equal (Kustas et al., 2003; Stewart et al., 1994); iii) there is no unique relationship between surface roughness characteristics such as the geometry of the roughness elements and z_{0H}, the roughness length for sensible heat (Brutsaert & Sugita, 1996; Lhomme et al., 2000; Schmugge et al., 2002; Stewart et al., 1994; Suleiman & Crago, 2002); iv) small errors in either T_{sR} or T_a will lead to large errors in the magnitude and even sign of H as a result of the relative sizes of ρc_p and R_a; v) H is very sensitive to fluctuations in R_a through its dependence on wind speed and atmospheric stability; vi) use of instantaneous measure of T_{sR} to calculate a time-averaged flux leads to errors. This is an issue for models using the MODIS 8-day T_{sR} which is a composite of once-daily overpasses at ~10:30 h local time, the time of overpass of the Terra satellite. As standard MODIS data processing procedures eliminate all cloud-contaminated periods (Wan et al., 2002), T_{sR} will be the average of between 0 and 8 values; and vii) T_{sR} is determined from a radiance measured by a sensor at the view angle at the time of overpass, and converted to a radiative temperature using emissivities based on vegetation classes using a 1-km grid that differs from the MODIS pixel location.

The models developed by Kustas and Norman (1999), and Su (2005) address these difficulties, but the resulting models are complex and hence unsuitable for routine delivery of a continental or global evaporation product. Therefore, we evaluate the simplest of the surface temperature-based models to test whether it is sufficiently robust and accurate for the task at hand.

2.2. Penman–Monteith model

We propose a fundamentally different approach to developing a satellite-based evaporation algorithm that uses the well-known Penman–Monteith (hereafter P–M) equation. Monteith (1964) eliminated surface temperature from Eqs. (1)–(3) to give:

$$\lambda E = \frac{sA + (\rho c_p D_a / R_a)}{s + \gamma(1 + R_s/R_a)} \tag{5}$$

where $s = de^*/dT$, the slope of the curve relating saturation water vapour pressure to temperature, $D_a = e^*(T_a) - e_a$ is the water vapour pressure deficit of the air (humidity deficit) and $e^*(T_a)$ is the saturation water vapour pressure at air temperature. All inputs have been previously defined except for surface resistance, R_s, which is an effective resistance accounting for evaporation from the soil surface and transpiration from the plant canopy. The aerodynamic resistance, R_a, can be estimated from Eq. (4) using z_{0V} (the roughness length for water vapour) in place of z_{0H} although in practice the two are usually assumed to be equal.

Over extensive, moist surfaces when R_s approaches zero, or when $R_s \ll R_a$, Eq. (5) reduces to the equilibrium evaporation rate:

$$\lambda E_{eq} = \frac{sA}{s + \gamma} \tag{6}$$

which is limited only by available energy. Raupach (2001) demonstrates why (6) is the theoretical upper limit for regional evaporation from land surfaces where moisture availability is not constrained. Conversely when $R_a \ll R_s$, evaporation is largely controlled by the surface resistance and Eq. (5) then reduces to:

$$\lambda E_{R_s} = \frac{\rho c_p D_a}{\gamma R_s} \tag{7}$$

Others have used somewhat similar approaches. Nemani and Running (1989) combined a modified version of Eq. (7) with surface temperatures from NOAA–AVHRR and the normalised difference vegetation index (N_D). More recently Nishida et al. (2003) used the complementary evaporation model of Morton (1969) and discount functions (Jarvis, 1976) to account for the effect of environmental factors such as light, humidity and soil moisture on the surface resistance. Although their efforts were reasonably successful, the evaporation models (i.e. Morton's complementary model and Eq. (7)) are not as theoretically sound as the P–M model. For example, Morton's model can be shown to fail for aerodynamically rough surfaces where R_a becomes small; while (7), as already noted, is only appropriate when $R_a \ll R_s$.

The full P–M equation provides a more robust approach to estimating land surface evaporation because: i) it combines the

main drivers of evaporation in a theoretically sound way; ii) it provides an energy constraint on the evaporation rate; iii) it has been successfully used to both diagnose and predict land surface evaporation; and iv) modelled evaporation fluxes are not overly sensitive to any of the inputs, i.e. differentiation of λE shows that (independent) changes in any of the input terms (x) on the RHS of Eq. (5) yield a conservative change ($\mathrm{d}\lambda E/\mathrm{d}x<1$) in predicted λE. Actual sensitivities depend on the environmental conditions, but in general: λE is only sensitive to wind speed when surface conductances are high, and the sensitivity can be positive or negative depending on the value of the surface conductance; and sensitivity of λE to humidity deficit (available energy) increases (decreases) with the aerodynamic conductance. Thom (1975) provides a more extensive discussion about the sensitivity of the P–M equation to its inputs.

Despite its theoretical appeal, the routine implementation of the P–M equation is often hindered by requiring meteorological forcing data (A, T_a and D_a) and the aerodynamic and surface resistances (R_a and R_s). Radiation and soil heat flux measurements are needed to determine A; air temperature and humidity to calculate D_a; and wind speed and surface roughness parameters to determine R_a. These problems are not unique to the P–M equation, since A, T_a and R_a are also required by all of the approaches using radiative surface temperature and the surface energy balance to calculate λE, including the resistance–surface energy balance model.

Fortunately, the necessary inputs are measured at flux station sites and so our model validation can utilize these data. However multi-temporal implementation of the P–M model at regional scales requires routine surface meteorological observations of air temperature, humidity, solar radiation and wind speed. Stability corrections to R_a (Eq. (4)) must be neglected, although this is justified because the P–M equation is relatively insensitive to aerodynamic resistance – especially when $R_a \ll R_s$ and at daily timescales. Surface albedo and emissivities of the surface and atmosphere needed to determine A, and the aerodynamic roughness needed for R_a, can be derived from remotely sensed radiance data or from models such as those described in Section 5.

Determining the surface resistance, R_s, is much more difficult. For a fully closed canopy, where $\Lambda>3$, the surface resistance is the parallel sum of the leaf stomatal resistances, i.e. $R_s = \overline{r}_{st}/\Lambda$ where $\overline{r}_{st}$ is the mean stomatal resistance (e.g. Monteith, 1980) which can be measured directly using porometry. Models for estimating maximum stomatal conductance exist (Kelliher et al., 1995) but including the effect of limited soil water availability and stomatal physiology requires either a fully coupled biophysical model such as that by Tuzet et al. (2003) or resorting to the empirical discount functions of Jarvis (1976), which must be calibrated. Neither of these are appropriate for a land surface evaporation model that is to be implemented routinely across the globe at spatial resolutions of a kilometre. Determining a *surface* resistance for partial canopy cover is even more challenging with various dual source models proposed (e.g. Shuttleworth & Wallace, 1985) to account for the presence of plants and soil. Given the impediment that R_s presents to using the P–M equation, we propose a model for R_s using remotely sensed vegetation indices.

2.2.1. Surface resistance algorithm

To estimate the surface resistance at 1-km scales utilising MODIS composite data, we postulate that the remotely-sensed vegetation indices such as N_D and the derived measures of canopy cover such as Λ and fractional land cover (f_c), are an adequate surrogate for R_s. Thus, if there is sufficient soil moisture for vegetation to develop, this will be manifested as a signal in N_D, f_c or Λ on timescales that match plant growth, i.e. weeks to months rather than hours to days, as demonstrated in studies by Lotsch et al. (2005) and Zhang et al. (2004, 2005). The greater the soil moisture and green canopy cover, the larger the signal in these vegetation indices, and thus the lower the surface conductance, G_s (Denmead et al., 1996; Kelliher et al., 1995) (note that $G_s=R_s^{-1}$ and conductance or resistance are used below whenever convenient). Low values of G_s are expected at low Λ and when low levels of soil moisture limits evaporation, while G_s will be high for well-watered surfaces with high Λ. Based on this reasoning we propose a simple linear relationship between Λ and the surface conductance, G_s:

$$G_s = c_L \Lambda + G_{s,\min} \tag{8}$$

Eq. (8) applies more correctly to canopy conductance, G_c, than to surface conductance, but $G_c \rightarrow G_s$ when soil evaporation is small compared to transpiration and when $\Lambda>2$ (Kelliher et al., 1995). The model parameters c_L and $G_{s,\min}$ must be determined empirically; c_L is the mean surface conductance per unit leaf area index and $G_{s,\min}$ is the surface conductance controlling soil evaporation and the conductance through the leaf cuticle.

While Eq. (8) has not been proposed as an approach to model surface conductance, several authors have noted the correlation between Λ and N_D and soil moisture (e.g. Choudhury & Golus, 1988) and land surface evaporation (Seevers & Ottman, 1994; Szilagyi & Parlange, 1999; Szilagyi et al., 1998). These studies proposed models that were typically statistical in nature and did not utilise the biophysical framework provided by the P–M equation and the known relationships between leaf area and canopy conductance. While these approaches do not seem to have been taken up by the hydrometeorological community, perhaps because of their empirical nature, they do provide observational support to the hypothesis embodied in Eqs. (8) and (5). It remains to test the validity of these equations by comparing modelled and local-scale measurements of land surface evaporation.

3. Flux measurement sites

Fluxes of sensible and latent heat used in the model evaluation were measured over two strongly contrasting ecosystems. The first is a wet/dry tropical savanna located in

northern Queensland (Virginia Park, 19°53′00″S, 146°33′14″ E, elevation of 200 m ASL), the other is a cool temperate, broadleaved forest in south east New South Wales (Tumbarumba, 35°39′20.6″S, 148°09′07.5″E, elevation of 1200 m ASL). Complete site descriptions, including the soil, rainfall climate and flux station measurements, are contained in Leuning et al. (2005).

Vegetation at Virginia Park consists of scattered *Eucalyptus creba* and *Eucalyptus drepanophylla* trees, 5–8 m tall and spaced ~30–40 m apart. A C_4 grassy understorey is present during the November to April summer wet season, but extensive grazing by cattle removes much of this during the dry season. This means that the canopy Λ varies from ~0.3 in the dry season to ~1.5 in the wet season. Rainfall was below the climatic average in the 3 years of measurement (Jul 2001–Mar 2004) with the last two wet seasons (2002–2003 and 2003–2004) in the lowest quartile, corresponding to a severe drought across much of eastern Australia. Mean daytime temperature during the measurement period was 25.1±5.3 °C (1 S.D.), with daytime humidity deficits ranging from 9.1 mmol mol^{-1} (June 2002) to 28 mmol mol^{-1} in the relatively dry summer of 2001–2002.

Vegetation at Tumbarumba consists of 40 m tall, *Eucalyptus delagatensis* and *Eucalyptus dalrympleana* wet sclerophyll forest, with Λ~1.4, while the understorey has a cover of shrubs and a full cover of grasses (Λ~1). Measurements at the Tumbarumba flux station reported in this paper span the period Feb. 2001 to Mar. 2004, ranging from an above average rainfall year (2001) to a severe drought from Mar. 2002 to May 2003. Mean daytime air temperature at the flux station was 10.0±7.0 °C, and daytime humidity deficits ranged from a low of 2 mmol mol^{-1} in winter (Aug. 2001) to 16 mmol mol^{-1} in mid summer (2003 and 2004).

Fluxes were measured using the eddy covariance technique. Instruments at Virginia Park were mounted at a height of 28 m, ~23 m above the zero-plane displacement (d) while those at Tumbarumba were located at 71 m above the ground, ~40 m above d (Leuning et al., 2005) These measurement heights were possible because of large upwind fetches (>1 km) of similar vegetation in each case. Sensible heat fluxes were measured with a Solent sonic anemometer (Model HS, Gill Instruments Ltd., Lymington, UK), while turbulent fluxes of water vapour and CO_2 were measured using the sonic anemometer and an open-path Licor 7500 sensor (Licor Inc., Logan, UT, USA). All sensors were logged at 20 Hz and fluxes were calculated using 1-hourly block-averages, with coordinate rotations calculated separately for each hour (Finnigan et al., 2003). Corrections to fluxes of CO_2 and water vapour due to density fluctuations introduced by the fluxes of sensible and latent heat were made according to Webb et al. (1980) and Leuning (2004).

Ancillary meteorological measurements needed for the analysis included net radiation, soil heat flux, soil temperature, air temperature and humidity and wind speed. Leuning et al. (2005) provide a detailed description of the sensors and their deployment. Missing meteorological data were interpolated using information from adjacent days and the meteorological data were used in a neural network analysis to fill gaps in the flux time series (Leuning et al., 2005). Daytime data for rain-free (but not cloud-free) periods were used in the analysis reported here to maintain consistency with the MODIS measurements. Meteorological and flux data from Tumbarumba and Virginia Park were averaged over the daylight hours and then further averaged according to the MODIS compositing periods.

The averaged measurements of available energy (A) and vapour pressure deficit (D_a) were used as inputs to both models (resistance–surface energy balance and P–M). R_a was estimated from flux tower wind speed measurements, using simple expressions for z_{0H} and d as a function of canopy height and no correction for atmospheric stability.

The following MODIS Collection 4 land data products were extracted from the FLUXNET website (http://www.fluxnet.ornl.gov/fluxnet/modis.cfm):

a) MOD11A2: 8-day, 1-km land surface temperature (T_{sR}, Wan et al., 2002);
b) MOD15A2: 8-day, 1-km leaf area index (Λ; Myneni et al., 2002);
c) MOD17A2: 8-day, 1-km gross primary productivity (P_G; Running et al., 2004);
d) MOD13A2: 16-day, 1-km vegetation indices (N_D, Huete et al., 2002).

The 1-km data were averaged over a 7×7 km^2 area centred on each flux tower to achieve spatial averaging and improve the representativeness of the data for each ecosystem. Analyses of the change in N_D and Λ as the cutout area is decreased from 7×7 km^2 to 3×3 km^2 confirm the homogeneity of the flux tower sites: N_D changed by an average of 0.02 (Tumbarumba) and 0.01 (Virginia Park). Changes in Λ were slightly larger: the average change resulting from shrinking the domain from 7×7 km^2 to 3×3 km^2 were 0.3 and 0.04 for Tumbarumba and Virginia Park, respectively. In part, this reflects the increase in uncertainty due to a poorer spatial sample for the 3×3 km^2 cutout. These changes are still less than 10% of the average Λ at both sites. All 8-day values were further averaged to match the 16-day periods used for the vegetation indices.

4. Results and discussion

4.1. Climatology and surface properties

Time series of T_{sR} and N_D for the 7×7 km^2 MODIS cutouts for Tumbarumba and Virginia Park are shown in Fig. 1. Gaps in the original record due to presence of persistent cloud cover during the wet season have been filled using linear interpolation, which may limit the validity of T_{sR} for the Virginia Park site in the first wet season (Dec. 2001–Feb. 2002). The N_D for Tumbarumba had a mean value of 0.80 for 2001–2003, with a fairly small annual amplitude ranging from a maximum of 0.89 (late autumn) to a minimum of 0.66 (late spring–early summer).

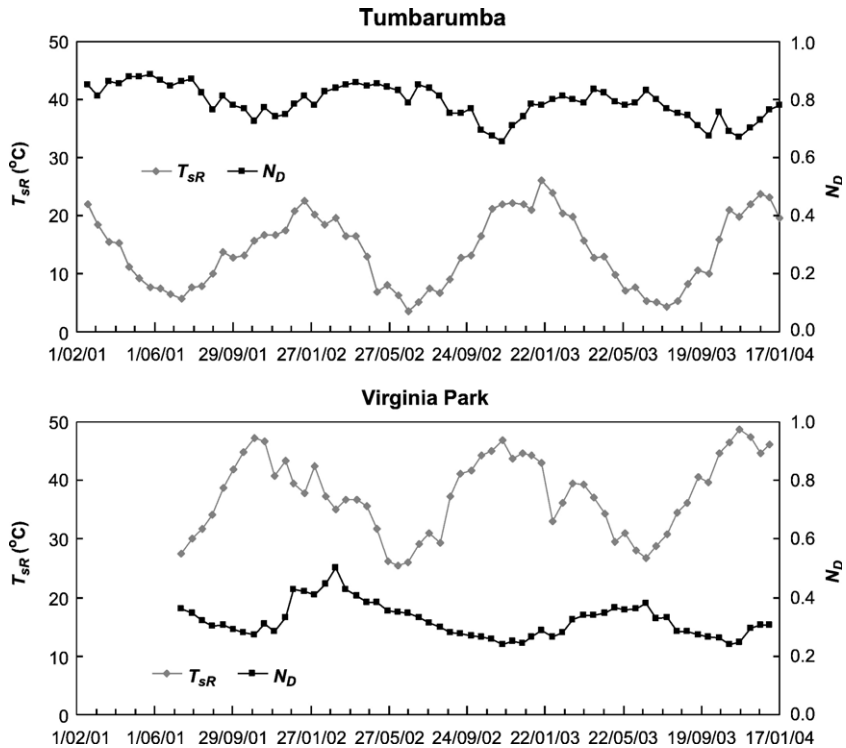

Fig. 1. Time series of MODIS N_D and T_{sR} (land surface temperature) for 7×7 km^2 areas surrounding the Tumbarumba and Virginia Park sites. Data are 16-day averages from 2001 to 2004.

The seasonal variation in N_D at Virginia Park depends mostly on the strength and timing of the wet season as this determines the flush of growth in the grass understorey. The peak value in N_D of 0.50 was recorded in March, 2002, demonstrating both the response of the canopy to the 2001–2002 summer wet season and the weakness of the subsequent wet seasons. Minimum N_D values of around 0.24 occurred in late spring to early summer (October–November) each year at the end of the long dry season. The average N_D at Virginia Park of 0.33 is less than half that of Tumbarumba.

MODIS land surface temperatures varied between 3 and 26 °C at Tumbarumba, significantly lower in magnitude, but similar in amplitude to the 25–48 °C range observed at Virginia Park. The peak surface temperature occurred in January at Tumbarumba, and towards the end of the dry season in November at Virginia Park, illustrating the influence of seasonal variations in solar radiation. The similarity in amplitude of the surface temperatures between the two sites contrasts with N_D, which showed less seasonal variation at Tumbarumba compared to Virginia Park. These differences in the phasing and magnitude mean that the relationship between T_{sR} and N_D at the two sites will be quite different.

4.2. Surface temperatures and sensible heat fluxes

As discussed in Section 2.1, T_{sA} is not generally expected to equal T_{sR}: T_{sA} is the aerodynamic surface temperature that satisfies the observed sensible heat flux (Eq. (1)), while T_{sR} is an instantaneous measurement that depends on the radiation balance of the surface elements at the time of the satellite overpass. These discrepancies are compounded by the non-linearity of Eq. (1) when using surface temperature products, such as MODIS, that are measured once daily and composited over 8- or 16-day periods. This is shown formally by the definition of the average value of the sensible flux over a period, t_A:

$$\overline{H} = \frac{1}{t_A}\int_0^{t_A}\left[\rho c_p \frac{T_{sA}-T_a}{R_a}\right]\mathrm{d}t. \tag{9}$$

The non-linearity of this equation means that

$$\overline{H} \neq \overline{\rho}\,\overline{c_p}\,\frac{\overline{T}_{sA}-\overline{T}_a}{\overline{R}_a} \neq \overline{\rho}\,\overline{c_p}\,\frac{\overline{T}_{sR}-\overline{T}_a}{\overline{R}_a}, \tag{10}$$

where the overbar represents the time-average. It is clearly incorrect to invert Eq. (10) to estimate $\overline{H}$ from the 8- or 16-day composites of surface temperatures. Further errors are expected because T_{sR} is measured only once per day by the MODIS instruments on the Terra and Aqua satellites.

To illustrate these points, 8-day composites of the MODIS T_{sR} are compared in Fig. 2 with T_{sA} calculated using Eqs. (1) and (4), with estimates of d and z_{0H} from relationships with canopy height and Λ (Raupach, 1994), and measured H, T_a and U for the 10:00–11:00 h period corresponding to the time of the Terra satellite

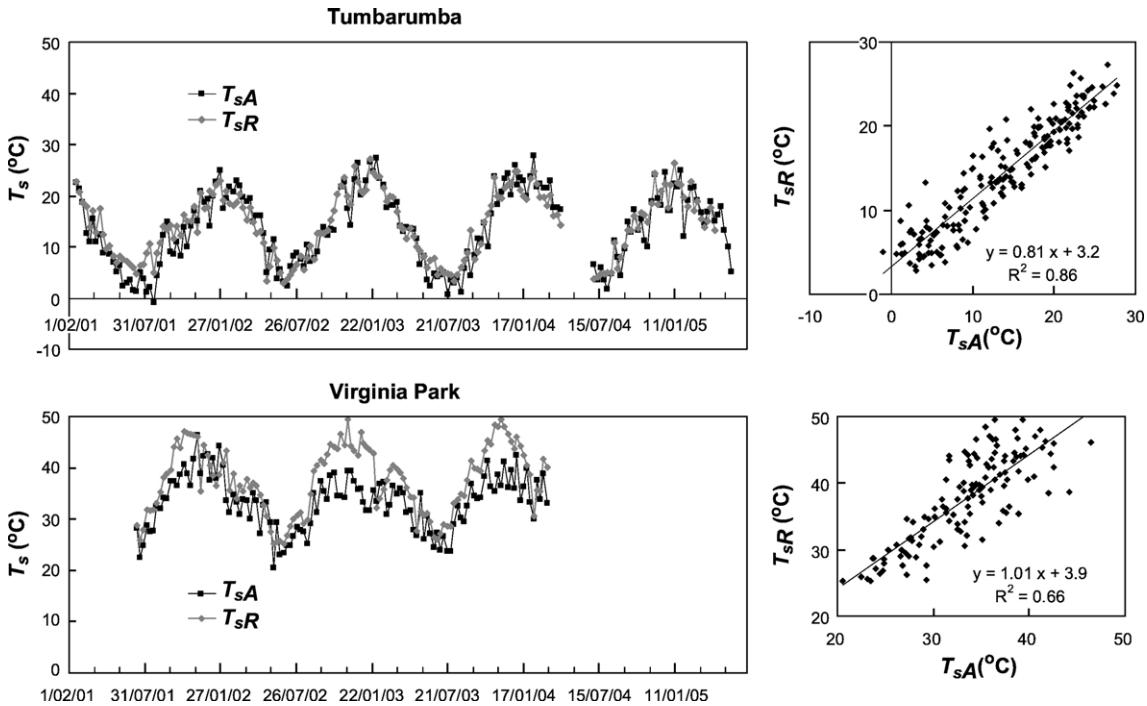

Fig. 2. Time series and scatter plots of T_{sR} (land surface temperature) from MODIS and T_{sA} (aerodynamic surface temperatures) calculated at Tumbarumba and Virginia Park. Data are 8-day averages.

overpass. The time series and scatter plots in Fig. 2 show a strong correlation between T_{sR} from MODIS and T_{sA}. At Tumbarumba $|T_{sR} - T_{sA}|$ was mostly <3 °C over the 50 months of measurements, except for larger discrepancies (up to 8 °C) in winter 2001 when snow cover possibly influenced T_{sR}. The agreement between T_{sR} and T_{sA} was not as good at Virginia Park, with $|T_{sR} - T_{sA}|$ exceeding 10 °C during each dry season (Nov.–Mar.).

Fig. 3 illustrates the errors in sensible and latent heat fluxes that result from using $\overline{T}_{sR}$ in Eq. (10) when the inequalities in this equation are ignored. There is little agreement in both absolute fluxes and seasonal dynamics between modelled and measured 8-day composites of $\overline{H}$ and $\overline{\lambda E}$ for the period 10:00–11:00 h. Fig. 3 also illustrates the physically unreasonable evaporation fluxes estimated using the resistance–surface energy balance method.

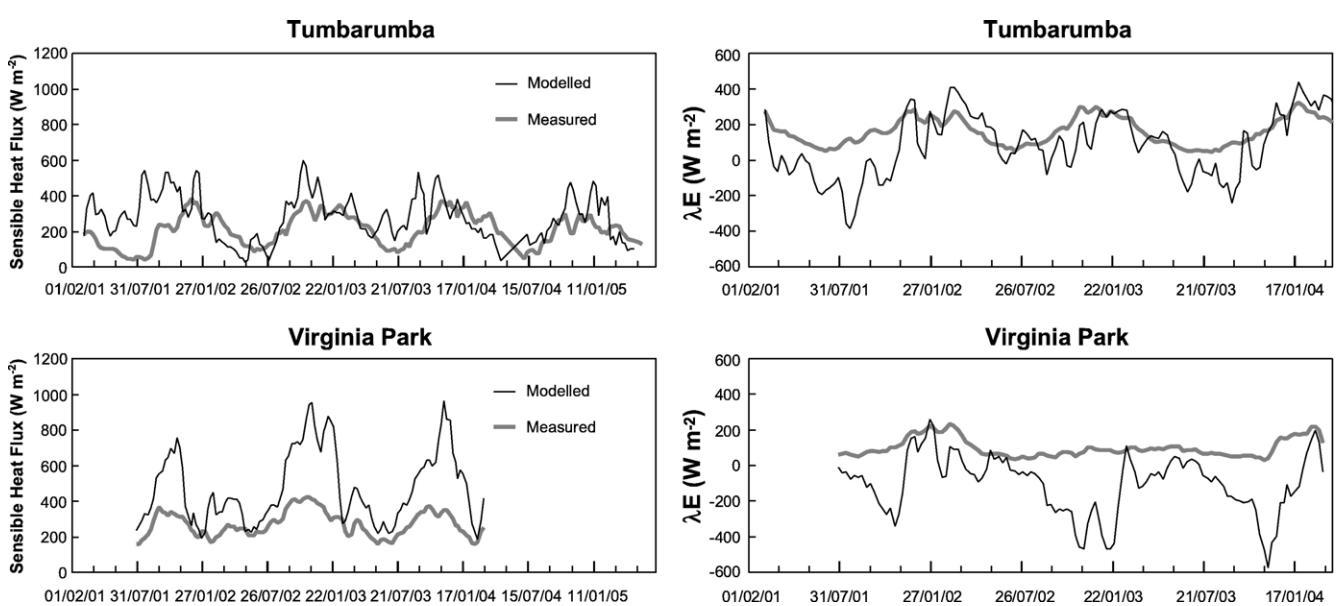

Fig. 3. Time series of measured and modelled: heat (H) and evaporation (λE) fluxes using the resistance–surface energy balance approach. Modelled fluxes use MODIS T_{sR} and all other inputs were measured at the Tumbarumba and Virginia Park flux towers. Data are smoothed 8-day averages from 2001 to 2005 and are for the period 10:00–11:00 h only.

Table 1
Statistics for the P–M model performance

Evaporation model	R^2	Slope	Intercept (W m^{-2})	$\overline{P}-\overline{O}$ (W m^{-2})	RMSE (W m^{-2})	Parameter values and description
1. Equilibrium evaporation	0.88	1.35	0.6	36.2	46.5	Tumbarumba
	0.23	0.55	134.2	105.3	112.1	Virginia Park
	n/a	n/a	n/a	66.9	98.4	Combined sites
2. Resistance–surface energy balance	0.41	1.73	−200.1	−86.74	200.1	Tumbarumba
	0.22	1.64	−267	−203.9	268.3	Virginia Park
	0.41	1.88	−257	−142.1	235.7	Combined sites
3. G_s from MODIS Λ and site specific c_L	0.74	0.89	8.6	−2.8	24.5	c_L=0.0019 (T) c_L=0.0025 (VP)
4. G_s from MODIS Λ and average c_L	0.74	1.01	0.69	−0.3	27.3	c_L=0.0022
5. G_s from MODIS Λ, time varying (Virginia Park only) and site specific c_L	0.77	0.93	2.89	−5.0	23.7	c_L=0.0019 (T) c_L=0.0025 (VP, winter) c_L=0.002 (VP, summer)

Unless otherwise indicated, both site datasets are combined. $\overline{O}$ and $\overline{P}$ are observed and predicted mean fluxes, where $\overline{O}$=85.5, 100.6 and 64.3 W m^{-2} for the combined and individual Tumbarumba and Virginia Park data sets, respectively. n/a indicates that it is inappropriate to combine the data sets from the two sites as they are separate populations.

Even for periods when there is close agreement between $\overline{T}_{sR}$ and T_{sA}, such as at Tumbarumba from January to June 2003, there are still large discrepancies between measured and modelled heat and evaporation fluxes. This demonstrates that even if it were possible to implement the model globally using a 1-day surface temperature product, large errors would arise that cannot easily be constrained using Eqs. (1) and (3).

This, and the model performance diagnostics shown in Table 1, demonstrates clearly that the resistance–energy balance approach does not perform well at the mesic Tumbarumba site and is very unreliable for the savanna site at Virginia Park. Although the approach may be applicable if surface temperatures are measured more frequently and are assimilated into a full surface energy balance model where the nature of the surface and parameters describing the surface are well known, we conclude that the resistance surface energy balance model does not meet the specifications defined in the Introduction and so is not appropriate as an ET algorithm for global implementation.

4.3. Evaporation estimates from the P–M equation

Estimates of λE at Tumbarumba and Virginia Park were made using the P–M equation, where G_s was calculated using Eq. (8) with $G_{s,min}$=0 and the MOD15A2 leaf area index product. Unlike the above analysis for the resistance–energy balance approach, the meteorological inputs here are averaged over daytime hours (non-rain days) and then over the 16-day compositing period used to determine MODIS N_D.

The value for c_L used in Eq. (8) was first optimised using the MOD15A2 value for Λ at each site. Optimum values of c_L for Tumbarumba and Virginia Park were quite similar, 0.0019 and 0.0025 respectively, despite large differences in vegetation and climatology between the two sites. The time series of evaporation predicted with the optimised values of c_L are in good agreement with measured fluxes (Fig. 4)) in terms of both

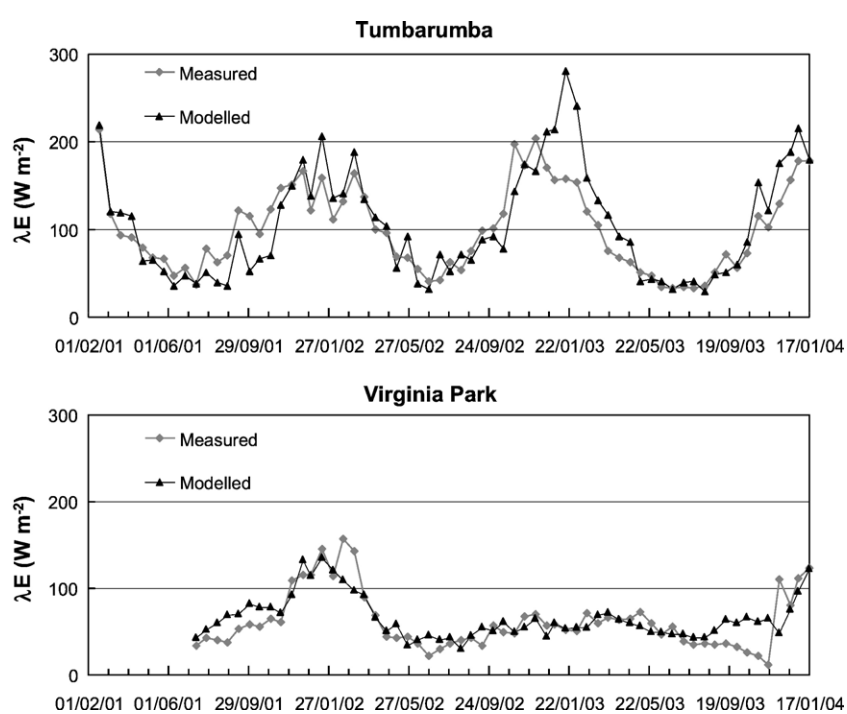

Fig. 4. Time series of measured and modelled λE, using the P–M model with G_s calculated from MODIS Λ and site-specific values of c_L.

the seasonal variation and magnitude. The main discrepancies occur in the very dry summer of 2002–2003 at Tumbarumba, when large vapour pressure deficits (Leuning et al., 2005) lead to predictions of λE that are 100 W m^{-2} higher than measured. Modelled evaporation fluxes for Tumbarumba were also 30–50 W m^{-2} lower than measured in winter and spring of 2001. The phase shift between modelled and measured λE at Tumbarumba during this period is the type of bias that can be expected from maximum value compositing of N_D, and points to the potential to improve this approach through refinements to the MODIS processing algorithms. At Virginia Park, modelled evaporation was greater than measured in the winter–spring periods of 2001 and 2003 but the overall agreement is very good. Especially encouraging is the ability of the model to simulate the timing and magnitude of the increased evaporation, and enhanced surface conductance (not shown), when the wet season occurs at Virginia Park. The model also captures the strong contrast in the magnitude and timing of evaporation between the two sites, thus supporting the model for surface conductance based on Λ.

Using a site-specific value for c_L, the model explains 74% of the variance in the measurements for the two sites, combined, while the slope and intercept of the line of best fit are not significantly different from 1 and 0, respectively (Table 1). Even with an average c_L for the two sites, the model still explains 74% of the variance, the slope of the regression between modelled and observed λE increases from 0.89 to 1.01 while the intercept is reduced from 8.6 to 0.69 W m^{-2} (Table 1). The RMSE for both values of c_L is similar (~30 W m^{-2}) By comparison, the resistance energy balance model explained 41% of the variance for the combined data with a large slope (1.88) and unacceptable bias and RMSE (absolute values exceeded 200 W m^{-2}). While the equilibrium evaporation model (Eq. (6)) yields a higher R^2 than the P–M model at Tumbarumba (0.88 compared to 0.74), the equilibrium model is clearly inappropriate for a dry site such as Virginia Park where the surface conductance is reduced for large parts of the year. Fig. 5 presents scatterplots for the two variations of the P–M equation: (a) using an optimised value of c_L for each site and (b) using an average value of c_L. These plots illustrate the statistical analysis shown in Table 1 and the qualitative trends in Fig. 4.

4.4. Evaluation of evaporation models

The analyses and results presented in Sections 4.2–4.3 show that the resistance–surface energy balance model does not correctly predict the magnitude and time course of land surface evaporation, especially in drier ecosystems such as the savanna, and so it is a poor candidate for a land surface evaporation model that meets the criteria laid out in Section 1.

Evaporation estimated using the P–M model, with a linear surface conductance model and the MODIS Λ product, matched both the temporal variation and magnitude of measured evaporation fluxes. Further tests of the P–M model were performed using a seasonally varying c_L at Virginia Park, acknowledging the large changes in vegetation cover between the wet and dry seasons in savannas, but this did not significantly improve the model predictions (Table 1).

Because of its superior model performance and the potential for constraining the estimates using energy conservation, we conclude that the P–M – MODIS approach has considerable potential for estimating weekly land surface evaporation at regional and global spatial scales. None of the more traditional models, based on multi-temporal thermal imagery, met all of the criteria listed earlier.

The tasks needed to realise this potential of the P–M model are described in Section 5, *viz*: i) acquiring the meteorological forcing at larger spatial scales through developing and testing sub-models for available energy (A), vapour pressure deficit (D_a), and R_a; ii) assessing the model performance when forced with these data; iii) implementing and assessing the model at regional and continental scales; and iv) testing the surface conductance algorithm over a more diverse range of ecosystems.

5. Implementing P–M at regional scales

5.1. Using non-local meteorological forcing

The above results suggest that the P–M model is the most appropriate model but these results were achieved using locally measured meteorological forcing. The next step is to investigate model performance when these local measurements are replaced by inputs derived from calibrated functions, broader scale

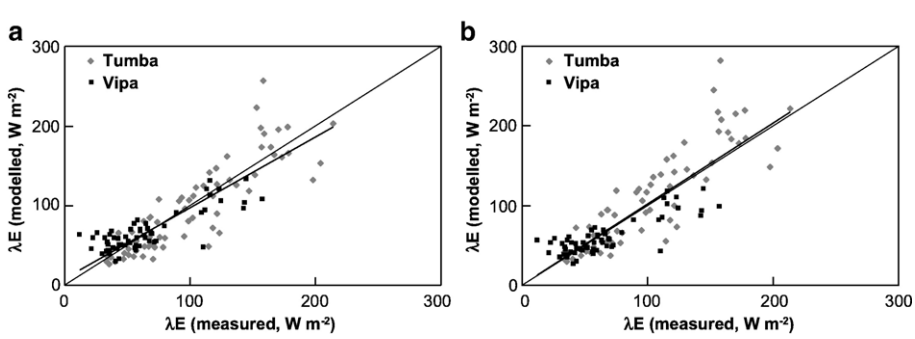

Fig. 5. Scatter plots of measured and modelled λE using the P–M model where G_s is calculated from MODIS Λ with (a) a site-specific value of c_L and (b) an average c_L. Table 1 specifies the regression coefficients and model performance statistics.

meteorological data and look-up tables for parameters that vary with vegetation type. Daily values of incoming solar radiation, temperature and humidity are available from a variety of sources, including the interpolated meteorological fields from the Data Assimilation Office (DAO) of the U.S. and Australia's Bureau of Meteorology.

The most critical meteorological inputs for the P–M equation are D_a and A, while the sensitivity of the model to aerodynamic conductance is low when $G_a \gg G_s$ (for arid ecosystems such as Virginia Park) or when the evaporation rate is close to equilibrium (for temperate forests such as at Tumbarumba).

Comparisons with flux tower measurements show large discrepancies with the DAO estimates of D_a, especially at Virginia Park (Fig. 6a), and so we developed a model for D_a using either air temperature (T_a) or surface temperature (T_{sR}) as inputs (Granger, 2000). There is no clear biophysical basis for any particular relationship between D and T_a or T_{sR}, although the upper limit to water vapour pressure in air, e_a, is determined by the exponential dependence of the saturation water vapour pressure, e_a* on T_a, while the lower limit is often set by e_a* at the daily minimum temperature. Since $D_a = e_a^* - e_a$, these limits suggest an exponential relationship between D and either T_a or T_{sR}, i.e. $D_a = ae^{(bT_{a,sR})}$. This is confirmed by comparing in Fig. 6b measured $\overline{D}_a$ with $\overline{T}_a$ measured at the flux tower and with T_{sR} from MOD11A2, where the overbars indicate time-averages. $\overline{D}_a$ estimated from T_{sR} is too large at the savanna site in summer (Fig. 6a) and also fails to predict the large humidity deficits observed at Tumbarumba in the drought in the summer of 2002–2003 (not shown). Fig. 6c shows that the best agreement between measured and modelled $\overline{D}_a$ is obtained when the DAO daytime average air temperatures

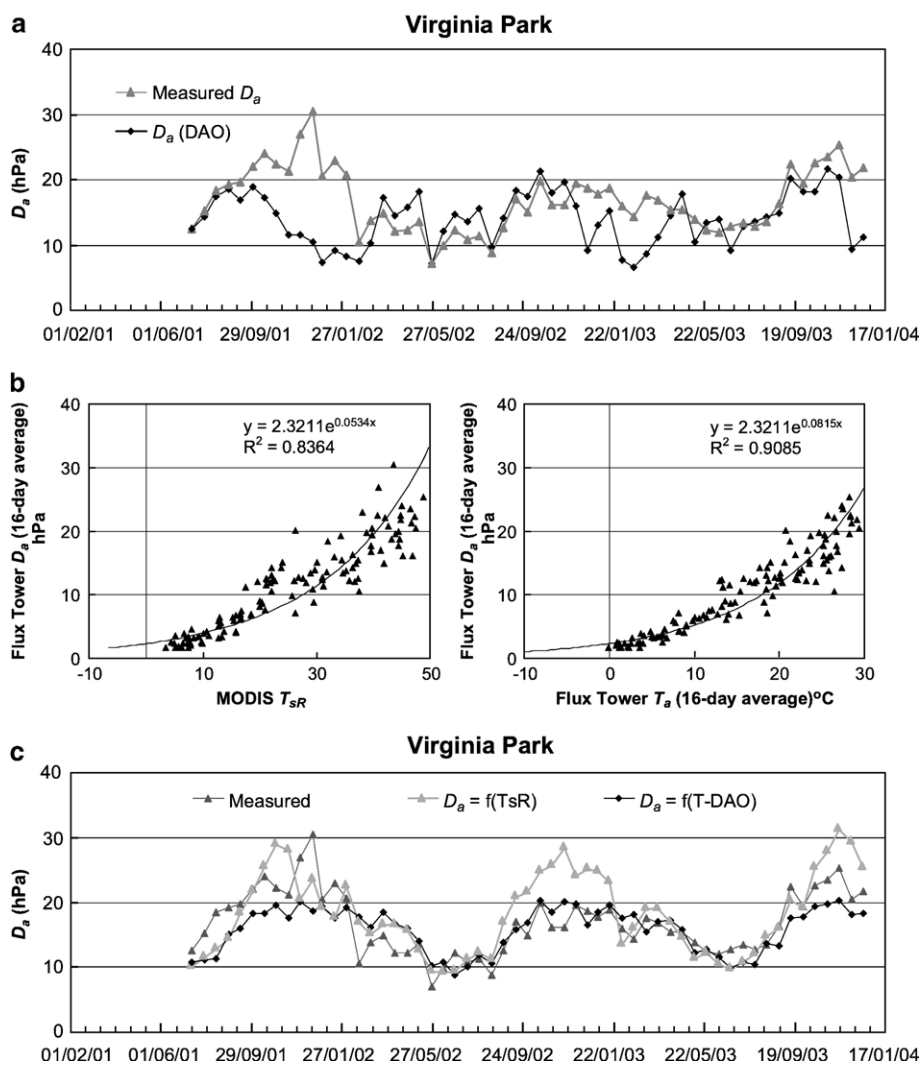

Fig. 6. (a) Time series of measured, 16-day average vapour pressure deficit (D_a) and the U.S. DAO values of D_a for Virginia Park; (b) 16-day average, measured D_a plotted as a function of MODIS surface radiative temperature (T_{sR}) and mean air temperature (T_a) measured at both flux stations; and (c) predictions using functions shown in (b), for Virginia Park only.

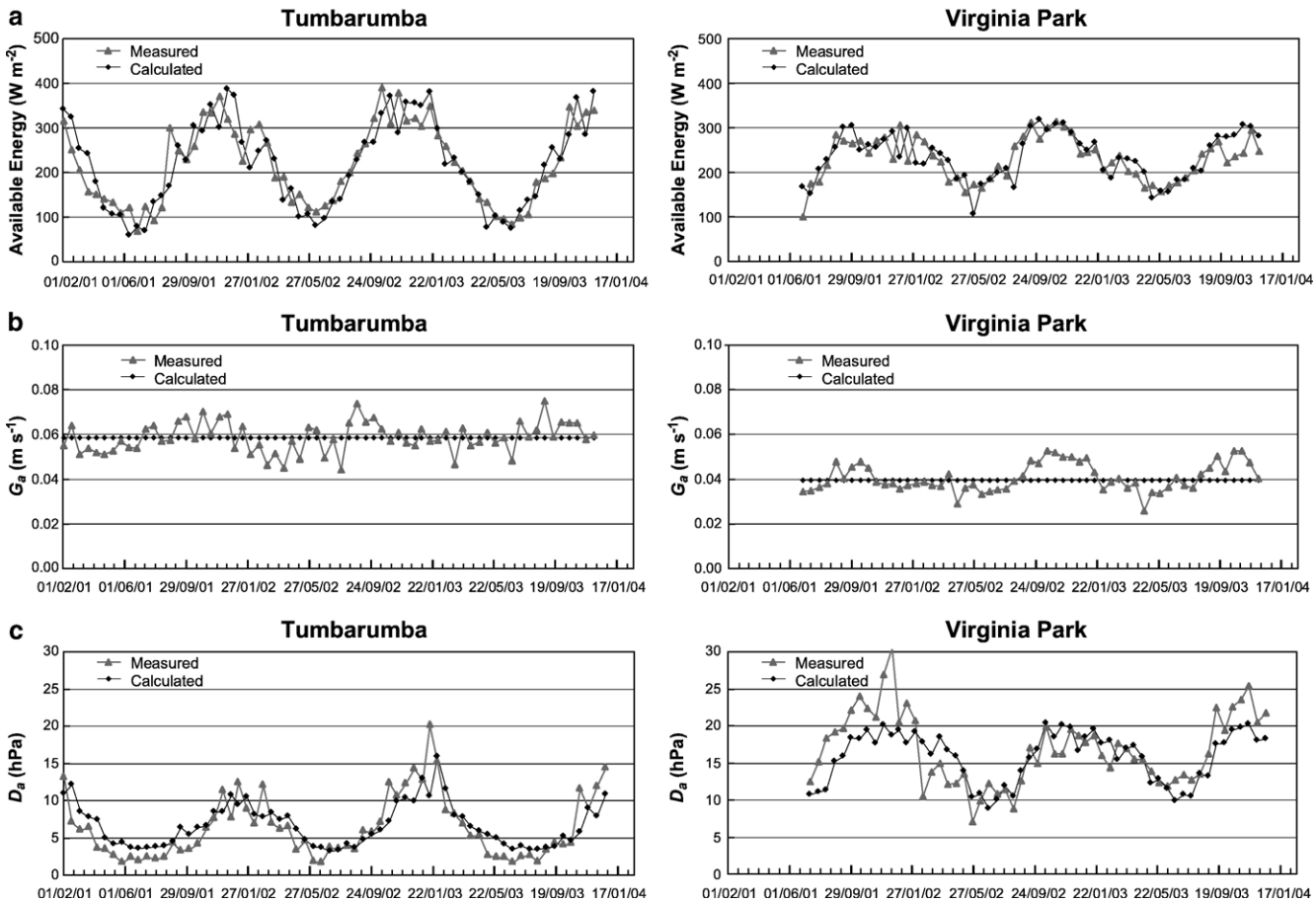

Fig. 7. Time series of measured and modelled values for (a) available energy, A; (b) aerodynamic conductance, G_a; and (c) vapour pressure deficit, D_a using the functions described in the text for Tumbarumba and Virginia Park.

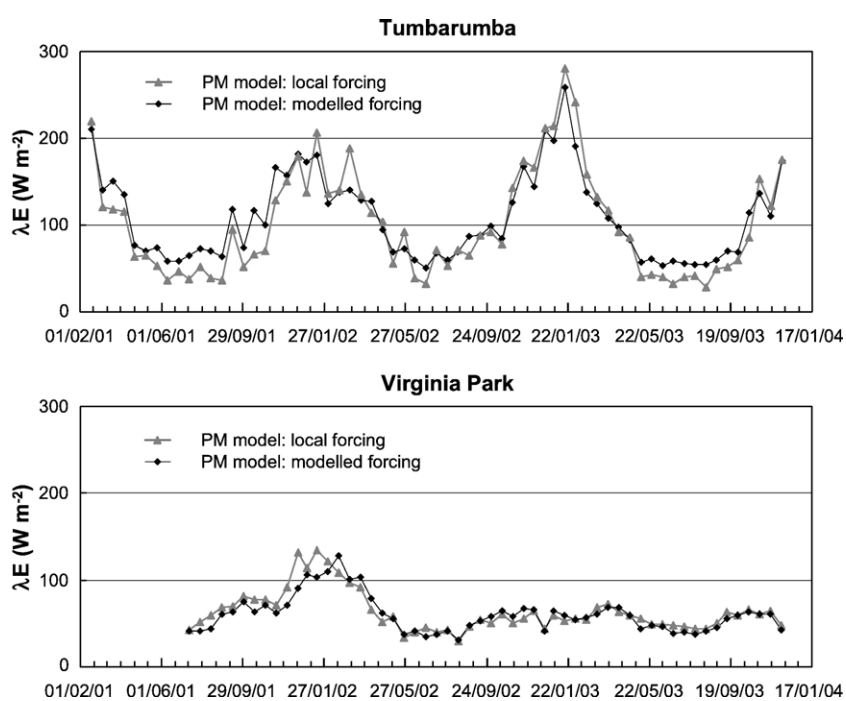

Fig. 8. Comparison between λE modelled using locally-measured inputs and MODIS Λ; and λE modelled using the functions shown in Fig. 9.

Table 2
Model statistics derived when the locally-measured inputs to the P–M equation are progressively replaced by values calculated from broader scale meteorological data (refer to text for further explanation)

Evaporation model	R^2	Slope	Intercept (W m^{-2})	$\overline{P}-\overline{O}$ (W m^{-2})	RMSE (W m^{-2})
1. Base model	0.73	0.98	6.3	4.9	27
2. A	0.71	0.96	7.5	4.3	28.1
3. D_a	0.78	0.89	15.5	6.6	22.8
4. G_a constant	0.71	0.98	6.3	4.8	28.1
5. ρc_p	0.73	0.97	6.8	4.3	26.7
6. All sub-models	0.74	0.89	15.7	6.7	24.7

$\overline{O}$ and $\overline{P}$ are observed and predicted mean evaporation fluxes. Note that the average period used is slightly shorter than for Table 1, and explains why the base model statistics differ slightly from Model 3 in Table 1.

($\overline{T}_{DAO}$) are used to predict the 16-day average humidity deficit via the relationship:

$$\overline{D}_a = 2.32e^{(0.082\overline{T}_{DAO})} \tag{11}$$

Available energy (A) is determined by separately computing the net all-wave radiation (R_n) and soil heat flux (G) components. From the radiation balance, R_n is the sum of the net shortwave and longwave radiation streams:

$$R_n = [S\downarrow(1-\alpha)] + [(\varepsilon_a-\varepsilon_s)\sigma T_a^4] \tag{12}$$

where $S\downarrow$ is the DAO estimate of shortwave radiation (MJ m^{-2} day^{-1}), adjusted for day length and α is surface albedo. The surface emissivity (ε_s) is assumed here to be unity but operationally, ecosystem classifications could be used to assign appropriate values. Atmospheric emissivity (ε_a) is calculated from air temperature using the formula of Idso and Jackson (1969):

$$\varepsilon_a = 1-0.261\exp[-7.77\times10^{-4}(273-T_a)^2] \tag{13}$$

with T_a is in K. Soil heat flux (G) is an assumed proportion (c_G) of the net radiation:

$$G = c_G R_n \tag{14}$$

While c_G can often be assumed to be negligible over these long time periods, at the savanna site better agreement with measured available energy was achieved by setting it to 0.1.

Fig. 7a and c show that the calculated inputs required by the P–M equation (A and D_a) closely match the absolute magnitude, range and temporal variability of the local measurements, with the exception of D_a at Virginia Park in the first year of measurements. Mean values of G_a appropriate to the aerodynamic roughness of each site were used to avoid detailed knowledge of the wind speed (Fig. 7b). Consequently, there was little change to estimates of λE from the P–M model when locally-measured meteorological forcing was replaced with calculated forcing using the DAO dataset, especially at Virginia Park (Fig. 8). Modelled meteorology caused λE to be overestimated at Tumbarumba by 20–30 W m^{-2} during the winter months in 2001 and 2003, but agreement was very good at other times.

Table 2 presents the model performance statistics derived when the locally-measured inputs to the P–M equation are progressively replaced by values calculated from meteorological data and the calibrated functions (Eqs. (11)–(14)). The base model results are the performance statistics for the P–M equation using locally-measured forcing, MODIS Λ and a site specific c_L

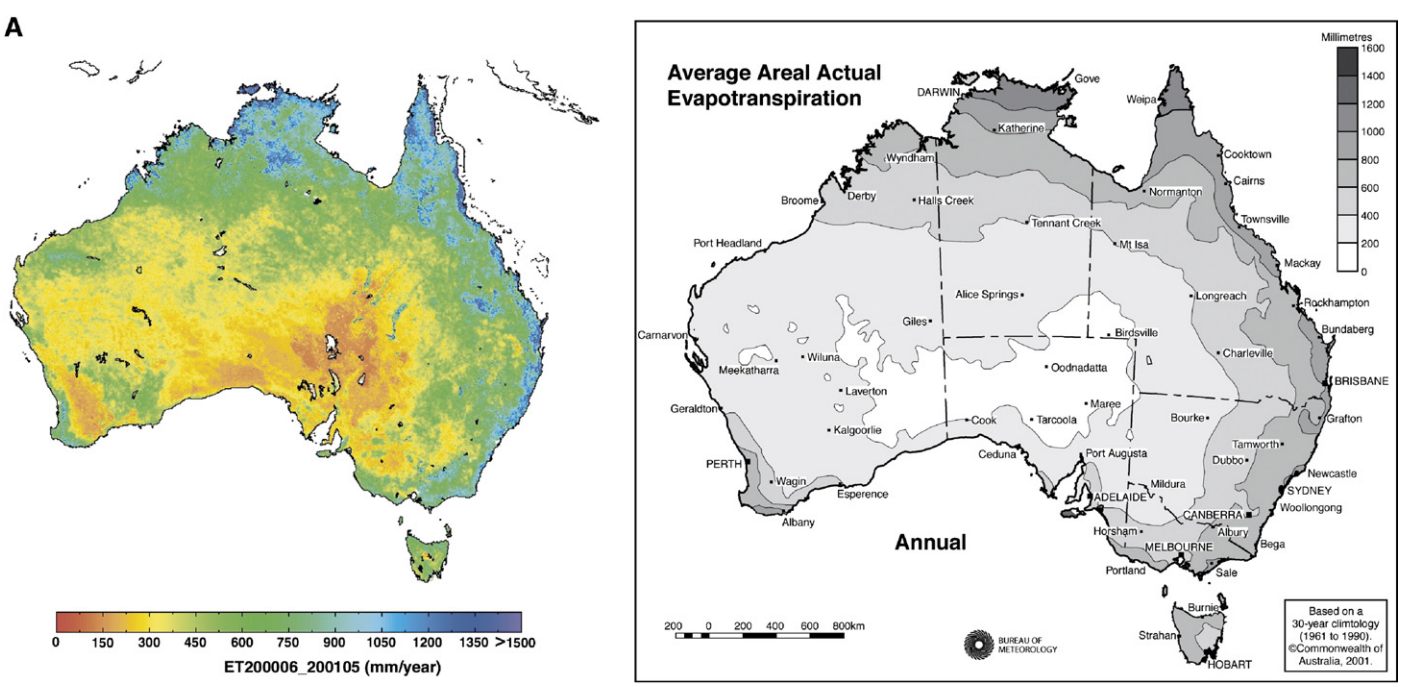

Fig. 9. Modelled land surface evaporation using P–M model and MODIS data (LHS) and climatological average estimated by Wang et al. (RHS): (a) annual total (mm year^{-1}); (b) mid summer (Jan., mm month^{-1}); and (c) mid winter (Jul. mm month^{-1}).

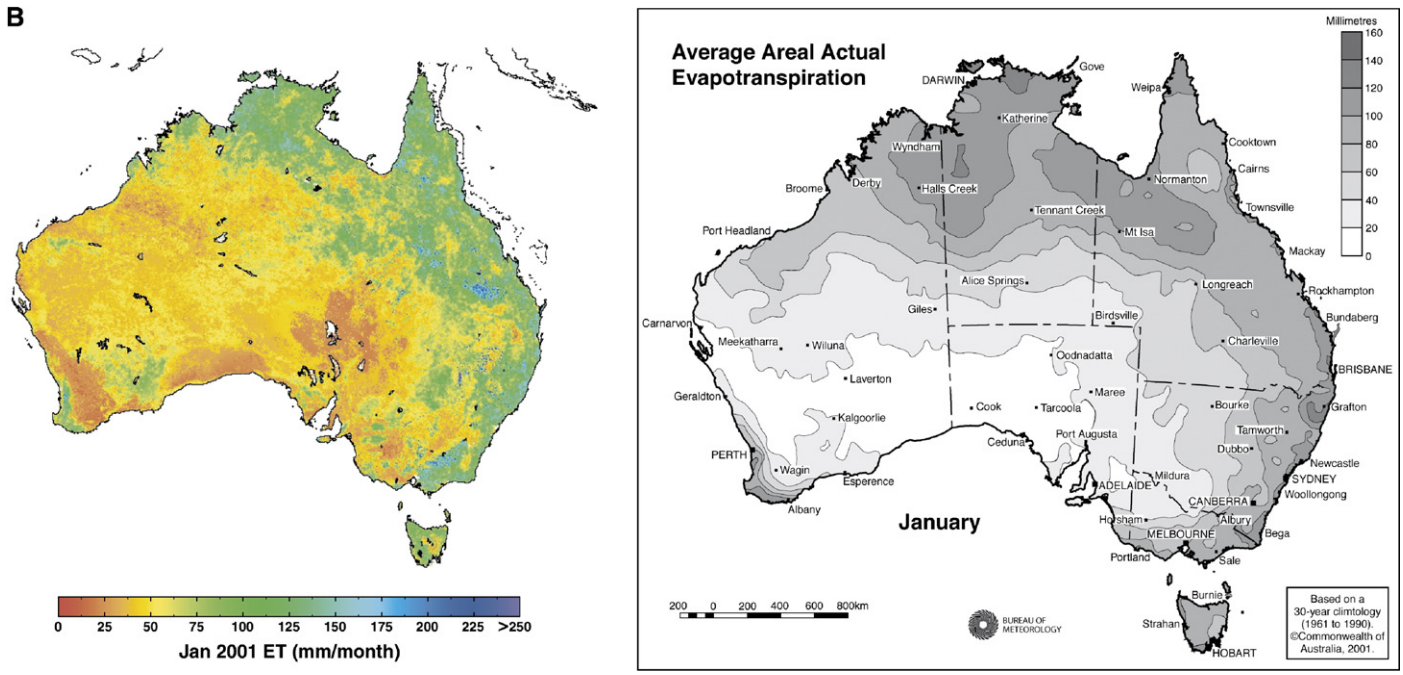

Fig. 9 (*continued*).

(i.e. Model 3 in Table 1). Subsequent rows show the result of progressively replacing each of the measured inputs (A, D_a, G_a and ρc_p) with modelled values derived using the sub models described in text. Table 2 shows that replacing all locally-measured inputs with modelled values leads to a slight improvement in R^2 (0.73 to 0.74) but the slope of the line of best fit drops from 0.98 to 0.89 and the intercept increases from 6.3 to 15.7 W m^{-2}. It is clear from the time series in Fig. 8 and the statistics presented in Table 2 that replacing locally measured inputs with values calculated from broader scale meteorological data and calibrated functions reduces model performance only slightly. This result reflects the relative lack of sensitivity of the P–M equation to any of the individual inputs.

5.2. Continental land surface evaporation climatologies

The above P–M approach is next used to estimate monthly land surface evaporation at 1-km resolution for Australia from 2001 to 2004. The MODIS products used to generate these spatial evaporation estimates are the 8-day, 1-km leaf area (Λ, MOD15A2), and the 16-day, 1-km normalized vegetation (N_D, MOD13A2) indices. Data were error-checked and erroneous values replaced with the preceding and subsequent values that meet the quality control criteria. These 8-day and 16-day products were then interpolated to provide daily values to calculate a daily surface conductance to match the daily timestep of the meteorological forcing data.

Daily, gridded meteorological data (solar radiation; vapour pressure; and daily minimum and maximum air temperature) were derived from the Australian Bureau of Meteorology's point measurements from their climate station network (about 700 stations for the period 2000–2004) and interpolated from 0.05° to 1-km using the thin plate splining and kriging techniques described in Jeffrey et al. (2001) and the following URL: http://www.nrm.qld.gov.au/silo/datadrill/datadrill_frameset.html. Atmospheric emissivity (ε_a) and humidity deficit (D_a) were calculated from the daily mean air temperature and Eqs. (13) and (11), and the aerodynamic conductance was fixed at 0.05 m s^{-1}. Available energy requires estimates of albedo and surface emissivity as well as solar radiation (Eq. (12)). A constant surface emissivity (0.97) was used while the continental albedo was determined using the data from Dilley et al. (2000) and Schaaf et al. (2002) and interpolated to 1-km resolution from the original 2.5° product.

These forcing data were used to compute daily land surface evaporation which was then aggregated to monthly, seasonal and annual averages for this analysis. While there are no measurements to validate these estimates, several consistency assessments can be made:

5.2.1. Seasonal variation in land surface evaporation

Fig. 9a (RHS) is an estimate of the climatological average (i.e. long-term) land surface evaporation across Australia that has been made available by Australia's Bureau of Meteorology (Wang et al., 2001[2]) using Morton's complementary evaporation model. It is the only other published evaporation product for Australia and is used here as a comparison for our MODIS estimates in 2001, when the rainfall was close to average. Such a comparison is between two modelled estimates of evaporation, where one is a long-term average, and so this can be no more than a qualitative consistency assessment.

The product of Wang et al. shows annual evaporation increasing from the south to the north, and from the interior to the

[2] http://www.bom.gov.au/climate/averages/climatology/evapotrans/et.shtml.

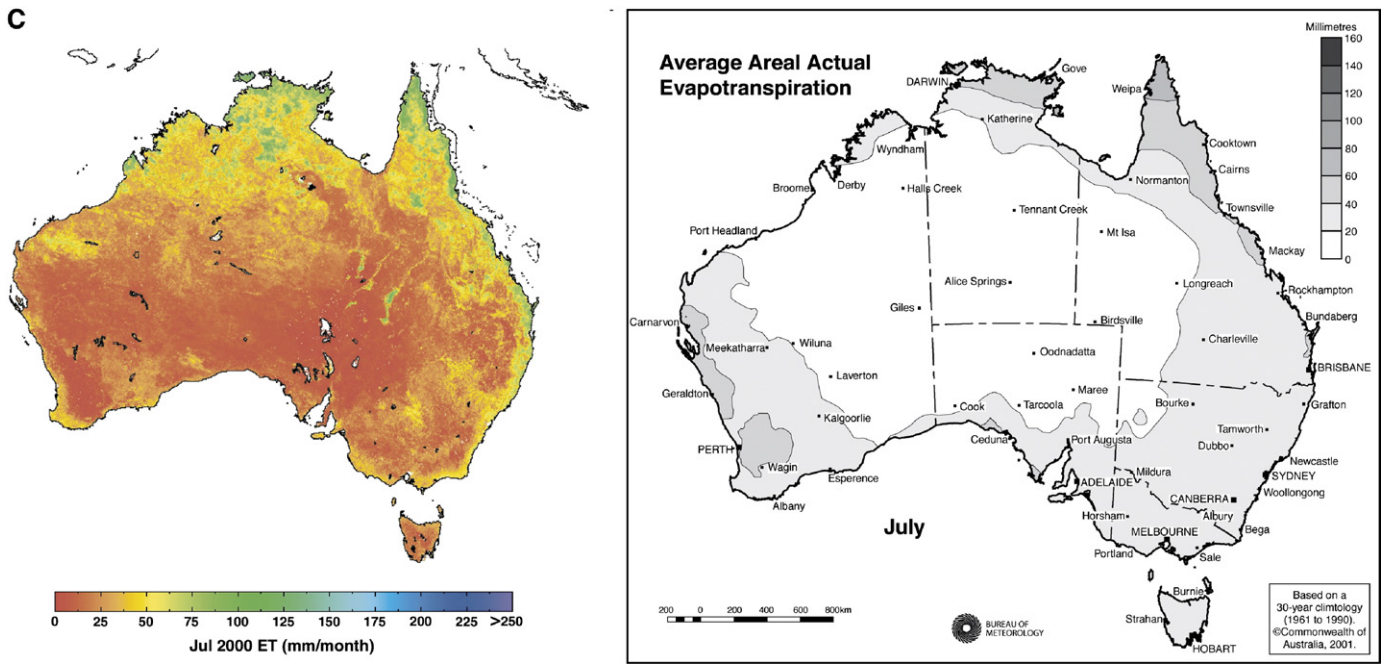

Fig. 9 (*continued*).

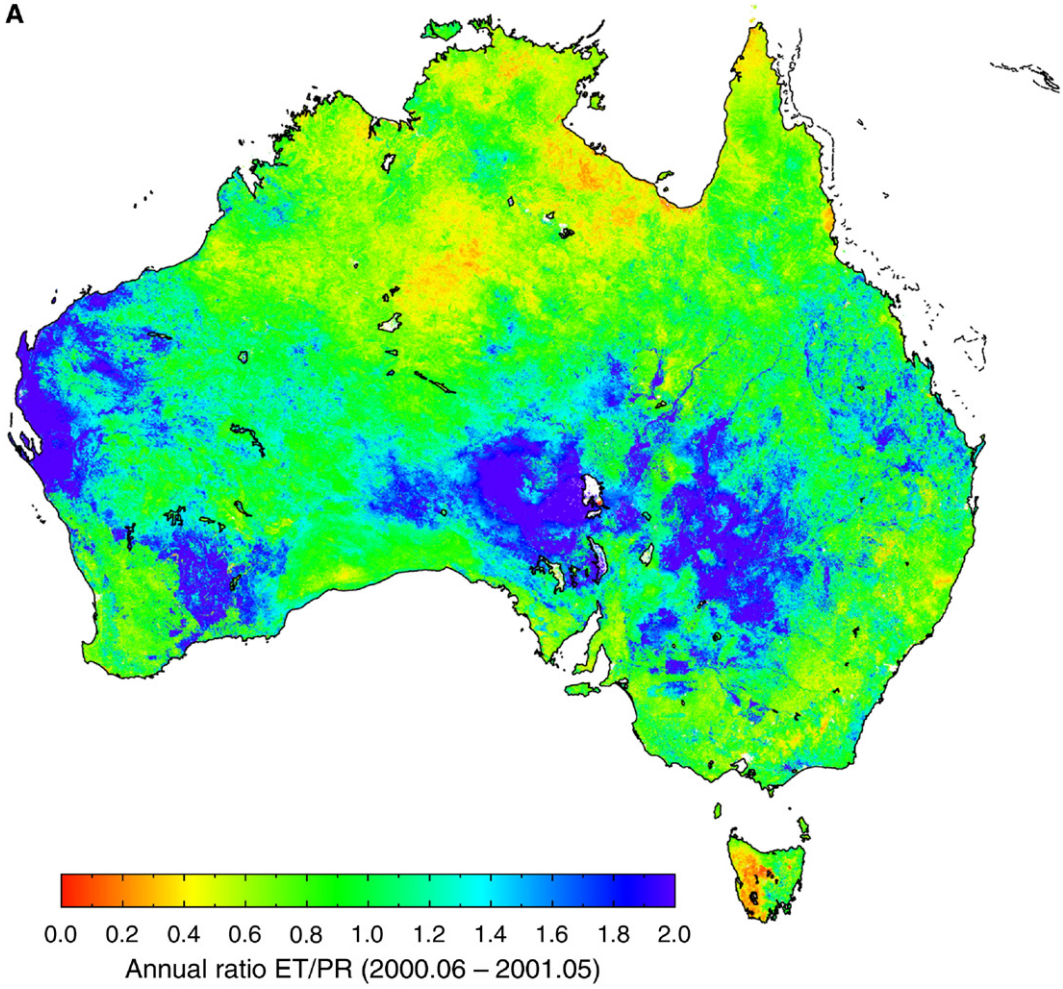

Fig. 10. Variation in the ratio of annual evaporation to rainfall (R_{ER}) for the Australian continent for the years 2000–2001 and 2001–2002. Evaporation was modelled using the P–M approach, while rainfall was obtained by interpolation of continental rainfall records.

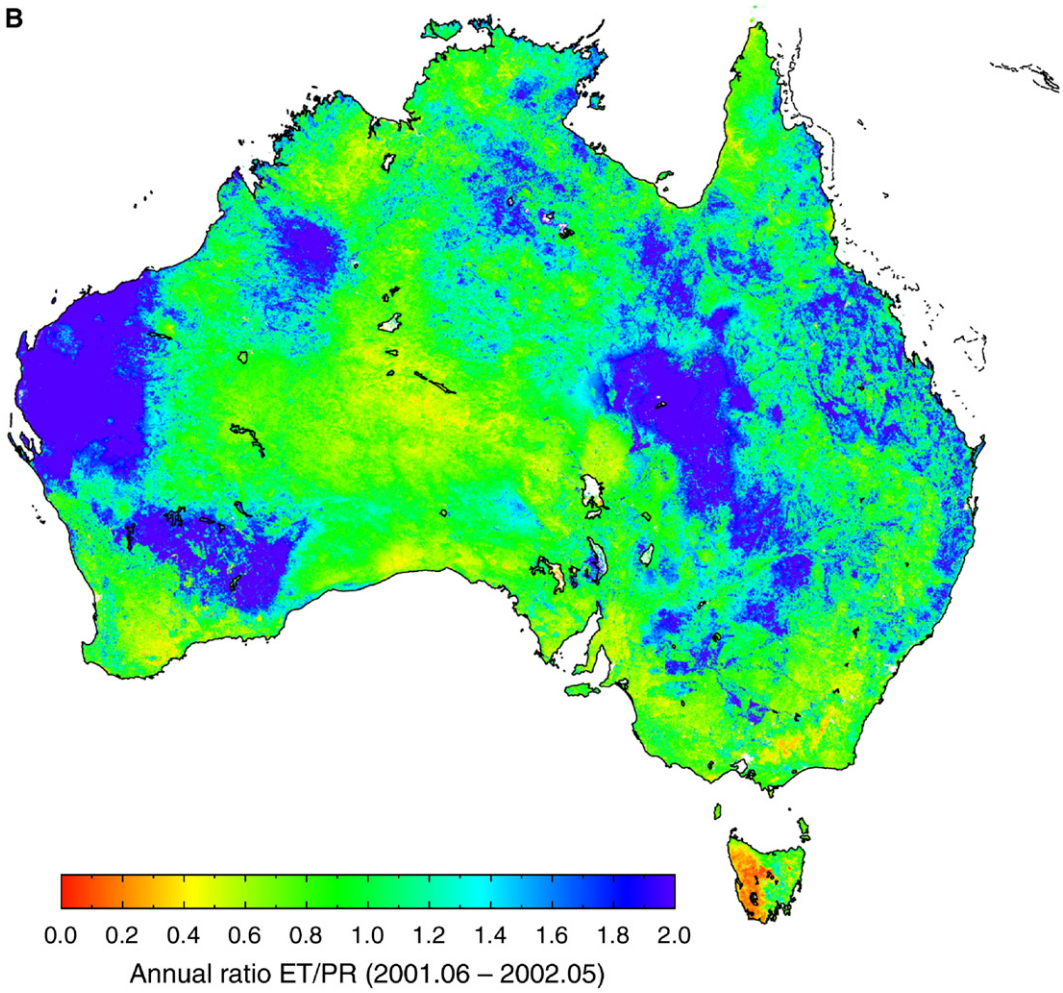

Fig. 10 (*continued*).

coast, reflecting variations in rainfall, available energy and temperature. These continental-scale evaporation trends are matched reasonably well by the MODIS estimates, i.e. the maximum annual evaporation rates in the north and around the east coast range from 1100 to 1400 mm year^{-1}, while the minimum rates in the southern interior are about 150 mm year^{-1} (Fig. 9a, LHS).

Both plots illustrate the magnitude and spatial pattern in summer evaporation (Fig. 9b): in the north and eastern parts of the continent evaporation rates peak at about 150 mm month^{-1} for January; there is a pronounced minimum of 20 mm month^{-1} in inland, SW Western Australia and a sharp gradient from this minimum to the SW coast; and a large crescent-shaped minima across the southern interior of about 20 mm month^{-1}.

Winter evaporation (Fig. 9c) shows much less variation across the continent in both plots, while the maximum and minimum evaporation rates and spatial trends are similar.

5.2.2. Seasonal and regional patterns normalised by energy and rainfall

Seasonal variations in land surface evaporation are quantified by two measures that also provide a physical upper constraint to land surface evaporation. The first is R_{ER}, the ratio of evaporation to rainfall. $R_{ER}=0$ means that all rainfall will be used to restore soil moisture or contribute to runoff, while $R_{ER}\geq 1$ means that all rainfall, and perhaps some stored soil water, contributes to evaporation. The second measure is $R_{PT}=\lambda E/\lambda E_{PT}$, the ratio of evaporation to the Priestley–Taylor (Priestley and Taylor, 1972) potential rate, defined as $\lambda E_{PT}=1.26\lambda E_{eq}$ (see Eq. (6)).

Fig. 10 shows the spatial distribution of R_{ER}. For 2000–2001, with rainfall close to or greater than normal, $R_{ER}\approx 1$ for much of the continent (Fig. 10a) with the notable exceptions being the "top end" and the areas coinciding with the great Dividing Range in eastern Australia and western Tasmania where R is closer to 0.4, indicating areas where runoff will be generated. The model predicts the unlikely result that $R_{ER}>1$ for the dry regions of central and NW Australia in each of the years shown in Fig. 10, but this is probably a numerical artefact caused by dividing very low rainfalls by small evaporation rates. In the following much drier year, the predicted R_{ER} has shifted towards the green and blue end of the scale across the whole continent (Fig. 10b), i.e. R_{ER} has increased from 0.4 to 0.6 in the runoff generating regions of the north and to about 1 in the east. This increase in R_{ER} reflects a reduction in rainfall

and/or an increase in evaporation. R_{ER} changed little in Tasmania, consistent with that region receiving close to normal rainfall across all 3 years.

Fig. 11a illustrates that for summer 2000–2001, modelled evaporation is close to the Priestley–Taylor potential rate ($R_{PT}=1$) in the far north and in the SE corner of the continent, while for much of the rest of the continent $R_{PT}>0.8$, indicating that λE equals or exceeds λE_{eq}. Predicted evaporation is slightly below equilibrium ($R_{PT}\approx 0.5$–0.7) in a thin strip around the coast of eastern Australia and Tasmania. The contrast with the much drier summer of 2002–2003 is quite clear (Fig. 11b) when R_{PT} declines to ~ 0.5 for those regions that were close to equilibrium in the north and SE of Australia in previous summer. In the winter months, $R_{PT}\geq 0.9$ for the southern fringes of the continent and Tasmania and around the equilibrium value of $R_{PT}\approx 0.8$ for much of the SE and SW regions (Fig. 11c), as expected for these regions that receive winter rainfall.

Although these modelled seasonal and spatial patterns are generally reasonable and consistent, it is almost certain that the estimates of land surface evaporation are incorrect for particular areas. Closer analysis of those locations where the seasonal variation in evaporation is known reveal likely errors in the MOD15A leaf area product and so a fruitful avenue for future work is to improve the MODIS algorithm for computing leaf area index for Australian ecosystems. Further testing of the algorithm, and the generality of the values of c_L used in this study, is also an important area of continuing work.

6. Concluding comments

Our goal was to develop a global model for monitoring land surface evaporation at weekly to monthly timescales and at 1-km to continental spatial scales using surface meteorology and MODIS remote sensing. We compared the remote sensing approach that uses radiative surface temperature to estimate evaporation with the P–M model. The resistance–surface energy balance approach yielded implausible and unrealistic estimates of evaporation. This approach failed because of the difficulties in using 8- or 16-day composites of once-daily measurements of radiative surface temperature, because of the inherent non-linearity in the governing heat transfer equation, and because there is no energy-balance constraint on the

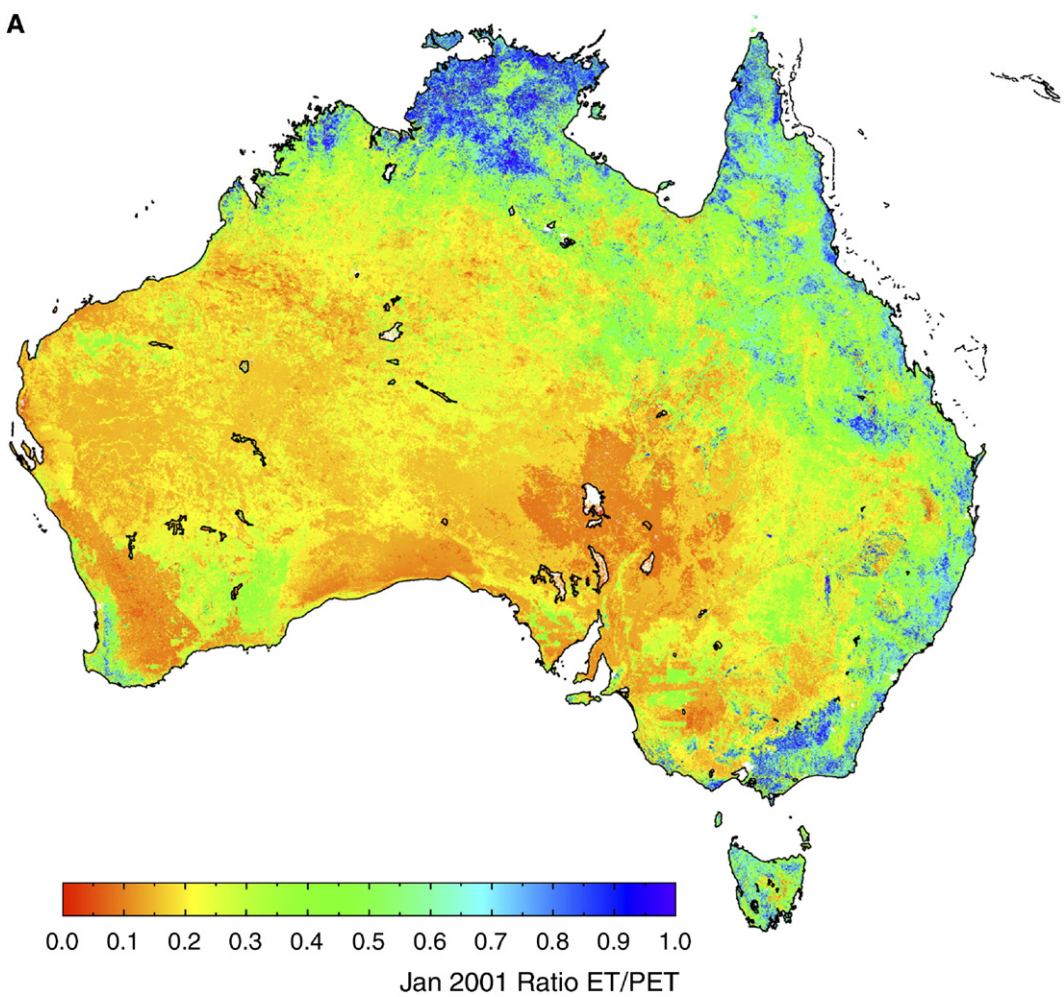

Fig. 11. Inter-seasonal variation in the ratio of predicted actual to potential evaporation (R_{PT}) for the Australian continent for (a) the average-rainfall summer of 2000–2001; (b) the dry summer of 2002–2003; and (c) winter 2000. Evaporation was modelled using the P–M approach, while potential evaporation was calculated using a model for net radiation and interpolated meteorological fields.

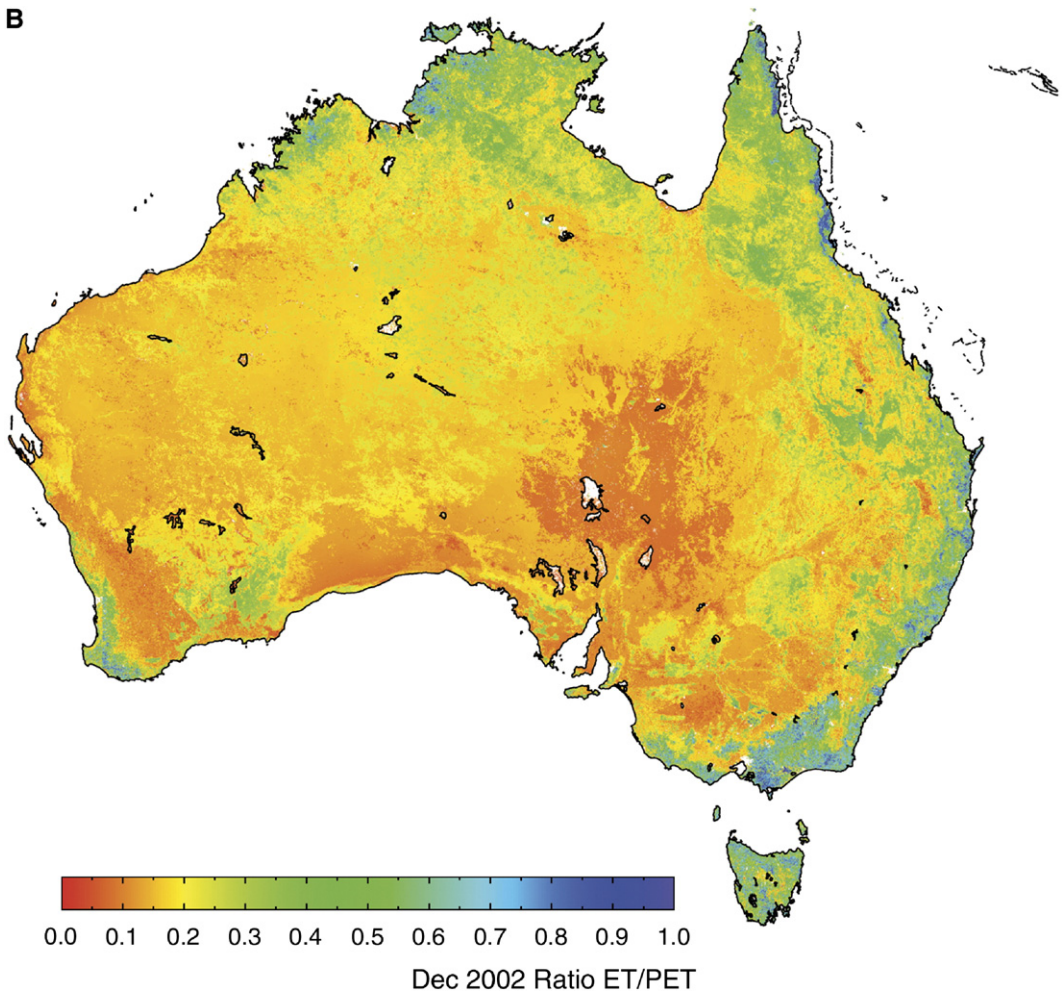

Fig. 11 (*continued*).

sensible flux derived from the radiative surface temperature. In contrast, evaporation estimates from the P–M model adequately matched the magnitude and seasonal variation in evaporation measured in two strongly contrasting ecosystems in Australia (a temperate forest and a grazed savanna), with a RMSE of 27 W m^{-2}. This error is comparable to other methods described in the literature for determining evaporation from satellite-based surface temperatures and vegetation indices: most methods have errors of ~1 mm day^{-1} (28 W m^{-2}) or 20–25%. None of these approaches has been developed for global implementation. The P–M approach is successful for this purpose because the calculated evaporation rates are inherently constrained by the surface energy balance, and are relatively insensitive to errors in each the four key driving variables: available energy, humidity deficit, surface resistance and aerodynamic resistance.

The innovative aspect of our P–M approach was to parameterise the surface conductance using a linear relationship with MODIS measurements of leaf area index. Optimising this conductance model using evaporation measurements reveals that the coefficients (c_L) are remarkably similar in value, despite the strong contrasts in vegetation and climate at each flux tower site, suggesting that the simple conductance equation has some general applicability. This has yet to be tested for a greater range of land covers and climatologies.

The simple parameterization for surface conductance resulted in close and unbiased agreement between estimated and observed evaporation over the 16-day periods used to composite the MODIS data. As the approach is intended for routine evaporation monitoring across large regions, at weekly to monthly time scales, it was necessary to use routinely observed or archived meteorological data to develop sub-models for available energy, humidity deficit, aerodynamic conductance, plus the thermodynamic parameters that are required by the P–M equation. Standard models are employed for net radiation that use measured albedo, incoming solar radiation and a standard expression for clear sky emissivity, while an empirical relationship using air temperature is developed for the humidity deficit. The agreement between these modelled and measured inputs is good and, importantly, the performance of the P–M model is only slightly degraded when it is implemented using these modelled inputs. These encouraging results are due to the theoretically sound basis of the P–M model and its relative insensitivity to errors in model inputs.

To demonstrate an intended application, we applied the model to the Australian continent using a 0.05° gridded meteorological

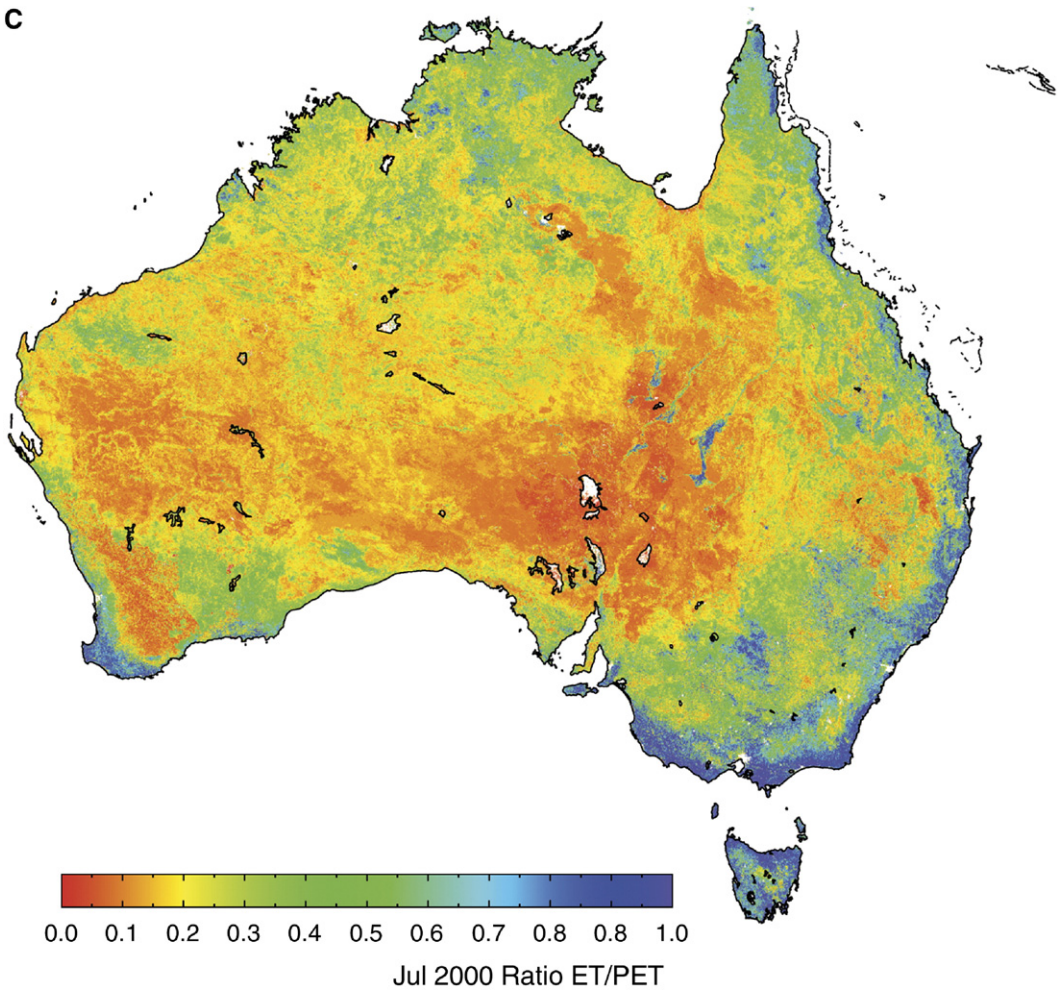

Fig. 11 (*continued*).

dataset and MODIS vegetation indices to provide a 3-year, monthly climatology of land surface evaporation.

The results of applying the P–M model at local and continental scales demonstrate that the approach: i) meets our specifications in terms of being robust across different ecosystems and climates, and performs well at the time and space scales of interest; ii) should be straightforward to apply to other land cover types through the use of look-up tables for key parameters. Two key sources of error lie in the simple surface conductance algorithm itself (both the linear relationship and the generality of the coefficient across all ecosystems) and the quality of the MODIS vegetation indices. Further research is needed to address these two issues.

Acknowledgements

The authors gratefully acknowledge the technical support given by Steve Zegelin, Dale Hughes and Mark Kitchen in the design, construction and maintenance of the flux stations, and to Christine Pierret for establishing the database used in processing the flux station results. We are also grateful to Faith Ann Heinsch for extracting the DAO meteorological fields for the Ozflux sites and the comments of Dr Damian Barrett (CSIRO Land and Water) on an earlier draft. This work was supported in part by a grant from the Australian Greenhouse Office (1999–2005) through the Australian Climate Change Science Program and its predecessors.

References

Baldocchi, D. D., Falge, E., Gu, L. H., Olson, R., Hollinger, D., Running, S., et al. (2001). FLUXNET: A new tool to study the temporal and spatial variability of ecosystem-scale carbon dioxide, water vapour and energy flux densities. *Bulletin of the American Meteorological Society*, *82*, 2415−2434.

Bastiaanssen, W. G. M., Menenti, M., Feddes, R. A., & Holtslag, A. A. M. (1998a). A remote sensing surface energy balance algorithm for Land (SEBAL): Part 1. Formulation. *Journal of Hydrology*, *212–213*, 198−212.

Bastiaanssen, W. G. M., Pelgrum, H., Wang, J., Ma, Y., Moreno, J., Roerink, G. J., et al. (1998b). The surface energy balance algorithm for land (SEBAL): Part 2. Validation. *Journal of Hydrology*, *212–213*, 213−229.

Brutsaert, W., & Sugita, M. (1996). Test of a sensible heat transfer parameterization for surfaces with anisothermal dense vegetation. *Journal of Atmospheric Science*, *53*, 209−216.

Caparrini, F., Castelli, F., & Entekhabi, D. (2003). Mapping of land–atmosphere heat fluxes and surface parameters with remote sensing data. *Journal of Hydrometeorology*, *5*, 145−159.

Choudhury, B. J, & Golus, R. E. (1988). Estimating soil wetness using satellite data. *International Journal of Remote Sensing*, *8*, 1085−1090.

Cleugh, H. A., & Dunin, F. X. (1995). Modelling sensible heat fluxes from a wheat canopy: An evaluation of the resistance energy balance method. *Journal of Hydrology*, *164*, 127−152.

Denmead, O. T., Dunin, F. X., Leuning, R., & Raupach, M. R. (1996). Measuring and modelling soil evaporation in wheat crops. *Physical Chemistry of the Earth*, *3*, 97−100.

Dilley, A. C., Edwards, M., O'Brien, D. M., & Mitchell, R. M. (2000). Operational AVHRR processing modules: Atmospheric correction, cloud masking and BRDF compensation.*CSIRO Atmospheric Research Paper*, *14* 24 pp.

Dodds, P., Meyer, W., & Barton, A. (2005). A review of methods to estimate irrigated reference crop evapotranspiration across Australia. *Technical Report 04/05, CRC for Irrigation Futures and CSIRO Land and Water, Adelaide, South Australia*.

Finnigan, J. J., Clement, R., Malhi, Y., Leuning, R., & Cleugh, H. A. (2003). A re-evaluation of long-term flux measurement techniques: Part 1. Averaging and coordinate rotation. *Boundary - Layer Meteorology*, *107*, 1−48.

Gillies, R. R., & Carlson, T. N. (1995). Thermal remote sensing of surface soil water content with partial vegetation cower for incorporation into mesoscale prediction models. *Journal of Applied Meteorology*, *34*, 745−756.

Granger, R. J. (2000). Satellite-derived estimates of evapotranspiration in the Gediz basin. *Journal of Hydrology*, *229*, 70−76.

Hall, F., Huemmrich, F., Goetz, S. J., Sellers, P. J., & Nikeson, J. E. (1992). Satellite remote sensing of surface energy balance: Success, failures, and unresolved issues in FIFE. *Journal of Geophysical Research*, *97*, 19,061−19,089.

Huete, A., Didan, K., Miura, T., Rodriguez, E. P., Gao, X., & Ferreira, L. G. (2002). Overview of the radiometric and biophysical performance of the MODIS vegetation indices. *Remote Sensing of Environment*, *83*, 195−213.

Idso, S. B., & Jackson, R. D. (1969). Thermal radiation from the atmosphere. *Journal of Geophysical Research*, *74*, 5397−5403.

Jarvis, P. G. (1976). The interpretation of the variations in leaf water potential and stomatal conductance found in canopies in the field. *Philosophical Transactions of the Royal Society, London B*, *273*, 593−610.

Jeffrey, S. J., Carter, J. O., Moodie, K. M, & Beswick, A. R. (2001). Using spatial interpolation to construct a comprehensive archive of Australian climate data. *Environmental Modelling and Software*, *16*, 309−330.

Kaimal, J. C., & Finnigan, J. J. (1994). *Atmospheric boundary layer flows: Their structure and management.* New York: Oxford University Press, 289 pp.

Kalma, J. D., & Jupp, D. L. B. (1990). Estimating evaporation from pasture using infrared thermometry: Evaluation of a one-layer resistance model. *Agricultural and Forest Meteorology*, *51*, 223−246.

Kelliher, F. M., Leuning, R., Raupach, M. R., & Schulze, E. -D. (1995). Maximum conductances for evaporation from global vegetation types. *Agricultural and Forest Meteorology*, *73*, 1−16.

Kustas, W. P., & Norman, J. M. (1999). Evaluation of soil and vegetation heat flux predictions using a simple two-source model with radiometric temperatures for partial canopy cover. *Agricultural and Forest Meteorology*, *94*, 13−29.

Kustas, W. P., Norman, J. M., Schmugge, T. J., & Anderson, M. C. (2003). Mapping surface energy fluxes with radiometric temperature. In D. A. Quattrochi & J.C. Luvall (Eds.), *Thermal remote sensing in land surface processes*. Taylor and Francis.

Leuning, R. (2004). Measurements of trace gas fluxes in the atmosphere using eddy covariances: WPL corrections revisited. In X. Lee, W. J. Massman, & B. E. Law (Eds.), *Handbook of micrometeorology* (pp. 119−132).

Leuning, R., Cleugh, H. A., Zegelin, S., & Hughes, D. (2005). Carbon and water cycles in two contrasting Australian ecosystems: Wet/Dry savannas and cool temperate *Eucalyptus* forest. *Agricultural and Forest Meteorology*, *129*, 151−173.

Lhomme, J. P., Chebouni, A., & Monteny, B. (2000). Sensible heat flux-radiometric surface temperature relationship over sparse vegetation: Parameterizing B^{-1}. *Boundary - Layer Meteorology*, *97*, 431−457.

Lotsch, A., Friedl, M., Anderson, B. T., & Tucker, C. J. (2005). Response of terrestrial ecosystems to recent Northern Hemispheric drought. *Geophysical Research Letters*, *32*. doi:10.1029/2005GL022952.

McVicar, T. R., & Jupp, D. L. B. (1999). Estimating one-time-of-day meteorological data from standard daily data as inputs to thermal remote sensing based energy balance models. *Agriculture and Forest Meteorology*, *96*, 219−238.

McVicar, T. R., & Jupp, D. L. B. (2002). Using covariates to spatially interpolate moisture availability in the Murray–Darling Basin: A novel use of remotely sensed data. *Remote Sensing of Environment*, *79*, 199−212.

Meyer, W. (1999). *Standard reference evaporation calculation for inland, south eastern Australia. Technical report*, *Vol. 35/98*. Adelaide, South Australia: CSIRO Land and Water.

Monteith, J. L. (1964). Evaporation and environment. *The state and movement of water in living organisms. Symposium of the society of experimental biology*, *Vol. 19* (pp. 205–234). Cambridge: Cambridge University Press.

Monteith, J. L. (1980). *Principles of environmental physics.* Edward Arnold.

Morton, F. I. (1969). Potential evaporation as a manifestation of regional evaporation. *Water Resources Research*, *5*, 1244−1255.

Myneni, R. B., Hoffman, S., Knyazikhin, Y., Privette, J. L., Glassy, J., Tian, Y., et al. (2002). Global products of vegetation leaf area and fraction absorbed PAR from year one of MODIS data. *Remote Sensing of Environment*, *83*, 214−231.

Nemani, R., & Running, S. W. (1989). Estimation of regional surface resistance to evapotranspiration from NDVI and Thermal_IR AVHRR data. *Journal of Applied Meteorology*, *28*, 276−284.

Nishida, K., Nemani, R. R., Glassy, J. M., & Running, S. W. (2003). Development of an evapotranspiration index from Aqua/MODIS for monitoring surface moisture status. *IEEE Transactions on Geoscience and Remote Sensing*, *41*, 493−501.

Norman, J. M., Kustas, W. B., & Humes, K. S. (1995). Source approach for estimating soil and vegetation energy fluxes in observations of directional radiometric surface temperature. *Agricultural and Forest Meteorology*, *77*, 263−293.

Priestley, C. H. B., & Taylor, R. J. (1972). On the assessment of surface heat flux and evaporation using large-scale parameters. *Monthly Weather Review*, *100*, 81−92.

Raupach, M. R. (1994). Simplified expressions for vegetation roughness length and zero-plane displacement as functions of canopy height and area index. *Boundary - Layer Meteorology*, *71*, 211−216.

Raupach, M. R. (2001). Combination theory and equilibrium evaporation. *Quarterly Journal of the Royal Meteorological Society*, *127*, 1149−1181.

Running, S. W., Baldocchi, D. D., Turner, D. P., Gower, S. T., Bakwin, P. S., & Hibbard, K. A. (1999). A global terrestrial monitoring network integrating tower fluxes, flask sampling, ecosystem modeling and EOS satellite data. *Remote Sensing of Environment*, *70*, 108−127.

Running, S. W, Nemani, R. R, Heinsch, F., Zhao, M., Reeves, M. C., & Hashimoto, H. (2004). A continuous satellite-derived measure of global terrestrial primary production. *Bioscience*, *54*, 547−560.

Schaaf, C. B., Gao, F., Strahler, A. H., Lucht, W., Li, X., Tsang, T., et al. (2002). First Operational BRDF, albedo and nadir reflectance products from MODIS. *Remote Sensing of Environment*, *83*, 135−148.

Schmugge, T. J., Kustas, W. P., Titchie, J. C., Jackson, T. J., & Rango, A. (2002). Remote sensing in hydrology. *Advances in Water Resources*, *25*, 1367−1385.

Shuttleworth, W. J., & Wallace, J. S. (1985). Evaporation from sparse crops – An energy combination theory. *Quarterly Journal of the Royal Meteorological Society*, *111*, 839−855.

Stewart, J. B., Kustas, W. P., Humes, K. S., Nichols, W. D., Moran, M. S., & de Bruin, H. A. R. (1994). Sensible heat flux-radiometric surface temperature relationship for eight semiarid areas. *Journal of Applied Meteorology*, *33*, 1110−1117.

Su, Z. (2002). The surface energy balance system (SEBS) for estimation of turbulent heat fluxes. *Hydrology and Earth System Sciences*, *6*, 85−99.

Su, Z. (2005). Hydrological applications of remote sensing. Surface fluxes and other derived variables–surface energy balance. In M. Anderson (Ed.), *Encyclopedia of hydrological sciences* : John Wiley and Sons.

Suleiman, A., & Crago, R. (2002). Analytical land–atmosphere radiometer model. *Journal of Applied Meteorology*, *41*, 177−187.

Szilagyi, J., & Parlange, M. B. (1999). Defining watershed-scale evaporation using a normalized difference vegetation index. *Journal of the American Water Resources Association*, *35*, 1245−1255.

Szilagyi, J., Parlange, M. B., Rundquist, D. C., & Gosselin, D. C. (1998). NDVI relationship to monthly evaporation. *Geophysical Research Letters*, *25*, 1753−1756.

Seevers, P. M., & Ottman, R. W. (1994). Evapotranspiration estimation using a normalized difference vegetation index transformation of satellite data. *Hydrological Sciences*, *39*, 333−345.

Thom, A. S. (1975). Momentum, mass and heat exchange of plant communities. In J. L. Monteith (Ed.), *Vegetation and the atmospherePrinciples*, *Vol. 1* (pp. 57−109). London: Academic Press.

Tuzet, A., Perrier, A., & Leuning, R. (2003). Stomatal control of photosynthesis and transpiration: Results from a soil–plant–atmosphere continuum model. *Plant, Cell and Environment*, *26*, 1097−1116.

Wan, Z., Zhang, Y., Zhang, Q., & Lim, Z. -L. (2002). Validation of land-surface temperature products retrieved from Terra Moderate Resolution Imaging Spectroradiometer data. *Remote Sensing of Environment*, *83*, 163−180.

Wang, Q.J, McConachy, F.L.N., & Chiew, F.H.S. (2001). Climatic atlas of Australia. Maps of evaporation. URL: http://www.bom.gov.au/climate/averages/climatology/evapotrans/text/et-txt.shtml

Webb, E. K., Pearman, G. I., & Leuning, R. (1980). Correction of flux measurements for density effects due to heat and water vapour transfer. *Quarterly Journal of the Royal Meteorological Society*, *106*, 85−100.

Zhang, X. Y, Friedl, M. A., Schaaf, C. B., & Strahler, A. H. (2004). Climate controls on vegetation phenological patterns in northern mid- and high latitudes inferred from MODIS data. *Global Change Biology*, *10*, 1133−1145.

Zhang, X. Y, Friedl, M. A., Schaaf, C. B., Strahler, A. H., & Liu, Z. (2005). Monitoring the response of vegetation phenology to precipitation in Africa by coupling MODIS and TRMM instruments. *Journal of Geophysical Research, [Atmospheres]*, *110*, D12103. doi:10.1029/2004JD005263.

Zhao, M., Heinsch, F. A., Nemani, R., & Running, S. W. (2005). Improvements of the MODIS terrestrial gross and net primary production global data set. *Remote Sensing of Environment*, *95*, 164−176.